SHAPE OPTIMIZATION OF A FAN DUNCTE FOR A VERTICAL TAKEOFF AND LANDING

by

JIE HUA

Presented to the Faculty of the Graduate School of

The University of Texas at Arlington in Partial Fulfillment

of the Requirements

for the Degree of

MASTER OF SCIENCE IN AEROSPACE ENGINNERING

THE UNIVERSITY OF TEXAS AT ARLINGTON

August 2018

Acknowledgements

I would like to express my very deep appreciation to my advisor Dr. Brian Dennis for giving me the opportunity to be a member of the CFD Lab at UTA, and inspiring me to CFD research. Without his help I cannot finish my research.

I am particularly grateful for Dr. Han and Dr. Bo. P. Wang for taking time to be my thesis committees, especially Dr. Han who gave me a lot of help during my academic year. I would like to thank Siddarth Chintamani, Sandeep Patel and Ashkan Akbariyeh for taking time with my thesis. Also I would like to thank Poudel, Kushal Raj and Gorla, Nishith who help me with the course problems.

I would like to express very great gratitude to my girlfriend Zhang, Jie who is always by my side. I would like to thank my parents who always support my every decision. I would like thank my roommates Alex Sanchez, Cameron and Alexis for helping me with daily life problem. I also grateful to my professor at undergraduate university who

At last, I would like to thank aircraft innovation laboratory and all my friends and colleges in China.

August 10, 2018

Abstract

SHAPE OPTIMIZATION OF A FAN DUNCTE FOR A VERTICAL TAKEOFF AND LANDING

Jie Hua, MS

The University of Texas at Arlington, 2018

Supervising Professor: Brian Dennis

The popularity of ride sharing services and recent improvements in electric car performance and automation have sparked interest in E-VTOL (Electric Vertical Takeoff and Landing) aircraft for personal transportation. Companies such as Uber, Airbus and EHANG are currently researching such aircraft for transportation over short distances in crowded urban environments. A personal E-VTOL design based on a ducted fan concept is proposed and the vertical lift capability is optimized. A numerical optimization algorithm is coupled with a computational fluid dynamics (CFD) analysis code to perform shape optimization. The objective is to determine the internal and external duct shape that maximizes the vertical force for a given fan speed. Different flow rates of the ducted fan and the propeller are considered. The shape is parameterized using b-splines with control points that are constrained to generate only valid shapes. Pointwise is used to automatically generate a hybrid mesh based on parameters generated by the optimizer. The mesh is then passed to FLUENT, which computes the flow field and calculates the vertical force achieved by the candidate design. The vertical force consists of the aerodynamic lift that is due to static pressure differences and force due to momentum

change that is generated by the ducted fan. Results are then passed back to the optimizer for use in generation of the next set of candidate design parameters.

Table of Contents

List of Illustrations

List of Tables

Chapter 1 Introduction

1.1 Requirement for E-VTOL

With rapid urban growth, traffic has become worse and worse. Every day, people spend millions of hours on road. Last year, the average San Francisco resident spent 230 hours commuting between work and home [1].In lot of global megacities, like Shanghai, most people spend almost 2 hours a day on road, so people are eager for alternate modes of transportation like aerial vehicles to improve urban mobility. In 1949, Taylor built the first 'production' Aerocar, which combined the car and fixed-wing, as showing in figure 1. However, the real first practical and production flying car is Transition, figure 2, designed by Terrafugia Company. However, several challenges need to be solved to make aerial vehicles a sustainable mode of urban transportation. Flying cars require runway, drivers need license to operate such vehicles and the problem of noise pollution need to be tackled.

Figure 1-1 Aerocar [2]

Figure 1-2 Transition [3]

Nowadays many companies such as Uber, Airbus and EHANG spend considerable amount of effort on researching E-VTOL (Electrical Vertical Takeoff and Landing) aircraft. Recent technological advances have made it practical to build such vehicles. A network of small, E-VTOL will enable rapid, reliable transportation between suburbs and cities and, ultimately, within cities [1]. E-VTOLs do not need runway. Buses,

trains, and cars take people from A to B along with limited routes. If there is any interruption, it will cause the serious delays. By contrast, E-VTOLs can travel toward their destination independently of any specific path with less prevalent [1], they can reduce the travel time from 1 hour to about 15minutes. By using electric motors and installing the autonomous systems, the VTOLs can become less noisy, produce lesser pollution, become more efficient, and eliminates the need for drivers to obtain license.

1.2 Temple VTOL Aircraft

The ideal of the VTOL aircraft started from Leonardo da Vinci's sketch book that has the first sketches of helicopter. Different designs have been developed to meet the demands for the VTOL Aircraft. This thesis does not talk about the VTOL technology that does not apply to the electric engine. The VTOL aircraft can be divided into seven categories: Helicopter, Tiltwing, Tiltrotor, Multirotor, Compound, Stock Tail and Ducted Fan.

1.2.1 Helicopter

Helicopter is the most widely used VTOL aircraft now. Its main rotor is the rotating wing, which provides the lift. The main rotor allows the helicopter to take off and land vertically, to hover, and to fly forward, backward, and laterally. Due to its good operating characteristics, helicopter can be used in complex areas where fixed-wing aircraft cannot perform. However, the main rotor generates the torque to the fuselage at the same time. So it needs device to provide the anti-force. According to different ways of generating anti-torque, there are five kinds of helicopters: Single main rotor with tail rotor helicopter, NOTAR, Tandem, Transverse, and Coaxial. There is another helicopter called tip-jet helicopter, its main rotor does not generate the torque. The most advantage of the helicopter is the efficiency due to the biggest disk area. However, the tip speed of the

rotor much faster can be transonic, so the shock reduces the efficiency, also the noise. Also the forward speed is not enough for many requirements.

Figure 1-3 BELL 407GXi [4]

1.2.2 Tiltrotor

In the late 1940s and early 1950s, the military wanted a kind of the VTOL aircraft which has higher forward speed and greater range than the helicopter. Bell Helicopter Company and Boeing designed tiltrotor XV-3, which was the prototype of V-22, the famous tiltrotor that is used today. The tiltrotor uses powered rotors or propellers to generate force for hover, the two rotating engine pods are mounted at the ends of wing. It has both the speed and range advantages of a fixed-wing aircraft and the hover capability of a helicopter. When operating at vertical flight condition, the two propellers rotate 90 degree from the horizontal state, so the shaft is vertical and generate lift like the helicopter rotor. When it flies forward, it is the same as the conventional fixed wing aircraft. Hover efficiency of the Tiltrotor is better than tiltwing. Since it just tilts the engines, the tilt force is less than tiltwing. But the flow from the propellers is against the wing. This reduces the propellers' efficiency. And the flow interferes with the wing and causes the wing flow to be unstable.

Figure 1-4 Bell Boeing V-22 Osprey [5]

1.2.3 Tiltwing

A tiltwing aircraft is different from a tiltrotor and has the propellers that are fixed in front of the wing. It rotates up entire wing rather than the engines for vertical takeoff and landing, but it also uses propeller to generate the lift which is similar to the tiltrotor design. Tiltwing has some advantages when compared with tiltrotor. Because the slipstream strikes the wing from propeller, the aircraft will lose some of its thrust due to this interference from the wing (V-22 for example loses about 10 percent). But since the tiltwing has less interference area, it can use more power to generate the lift. Also unlike the tiltrotor, the tiltwing can mount more engines as shown in figure 1-5. The drawback of the tiltwing is that the tilt wing has much greater surface exposed to the wind. This will cause the control problem.

Figure 1-5 Greased Lightning (GL-10) [6]

1.2.4 Mutirotor

Multirotor is a type rotorcraft with more than two rotors. The first prototype of multirotor was design in 1907 by Breguet brothers and their professor, but it was not very stable and just stayed airborne for a short time. After that some people also tried other designs, however due to the control problem, none was put into use. After 1990s, with the development of Micro-Electro-Mechanical System, multirotor became popular. Multirotor is easy to control by a processor, unlike the helicopter or fixed wing which are complex and require nonlinear control. It just needs to change the speed of each motor. Also, it is easier to construct making it the most widely used UAV. Depending on the number of motors it uses, it is called as tricopter, quadcopter, hexacopter and octocopter. The multirotor has less endurance time, and cannot carry much weight.

Figure 1-6 Multirotor

1.2.5 Multirotor and Fixed Wing Compound

This compound VTOL aircraft is easier to realize. It requires increasing the wing torque strength to add the multirotor into the fixed wing. And the flight control is also easier to realize, using two modes of control system which can be changed from time to time. The propeller is different for forward and vertical flight due the propeller coefficient. Unlike tiltwing and tiltrotor, they both use the same propellers, but this compound aircraft uses special propellers for different situations, so the propeller coefficient is great than

tiltwing and tiltrotors'. Although this design has some advantages, it has more drag and weight and cannot carry heavy payload.

Figure 1-7 Dronetech UAV AV-2 [7]

1.2.6 Stock Tail

Tiltwing and tiltrotor aircraft needs the design and the tilt mechanism to operate, which increases the weight. The stock tail aircraft does not need tilt mechanism, it stands whole aircraft for vertical flight, and tilt whole aircraft by actuator. In the 1950s, US navy built and tested a stock tail aircraft XFY-1, but due to some problems it was cancelled. One problem is that it needs highly skilled pilot. This design is hard to apply to aircraft, but it is good for applications such as the UAV which has less weight and do not need any pilots. Figure 1-8 shows personal VTOL design proposed by NASA.

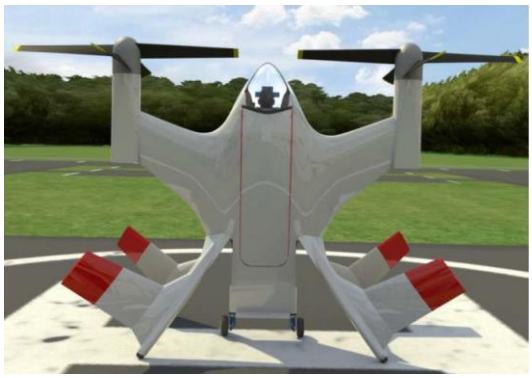

Figure 1-8 NASA Puffin electric VTOL [8]

1.2.7 Ducted fan

Compared to rotor and propeller, the ducted fan has more lift force at the same disk area because of the suction generated by leading edge of duct. Recently, many VTOL aircraft adopted the ducted fan to generate lift force. In the ducted fan, the propeller is inside of the duct and it would not hurt human, so it is safer, and the duct can reduces the noise of propeller. Normally, the ducted fan is placed at the center of gravity, so it does not have the balance problem, and the whole force of ducted fan can provide as the lift for aircraft. One company in Israel designed and tested the city VTOL which is the ducted fan VTOL aircraft, as shown in the figure 1-9. Currently, research on tilt ducted fan technology and ducted fan multirotor is being conducted. In the future, they may be realized. But the ducted fan has been less effective due to its smaller disc area, and greater electricity consumption when compared with the propeller.

Figure 1-9 City VTOL [9]

Chapter 2 Design

2.1 Design goal

This design goal is to create a single person E-VTOL, with a payload of 120 kg, with lower noise, safer, faster and more efficiency for traveling and shorter distance urban area commute, such as home to office or home to airport.

Compared to the current VTOL aircraft and helicopter, the new design should reduce the noise level significantly. And it also needs to be safe, so it should consider the distributed electric propulsion (DEP) technology. The range should be greater than maximum commuting distance of a metropolis, about 60 kilometer. The cruise speed should about 120 km/h, so it just needs 30 minutes to get anywhere in the city. The cruise altitude is about 1000 m that is enough for urban environment.

2.2 Preliminary Design

With the given requirements, the aircraft design can be broken into three major phases: they are conceptual design, preliminary design, detail design and test and evaluation [10]. The first step is conceptual design which is the most important phase of the design system. Conceptual design phase is decision-making process that does not contain any the precise calculations, such as which configuration should be chosen. At the preliminary design phase, it will decide some parameters and use some calculations or simulation. Though the parameters chosen are not the final decision, they directly influence detail design and are the essential parameters [10]. The last two phases are not considered in this work. So the design steps are estimating maximum take-off weight; choosing the way of VTOL and engine power; choosing configuration and deciding the parameters.

2.2.1 Gross weight estimation

Take off gross weight is the total weight of the aircraft. It contains the crew weight, payload weight (cargo weight and passenger weight), fuel weight and empty weight (landing gear, structure, engines, or others). Using equation to express [11]:

$$W_0 = W_{crew} + W_{payload} + W_{fuel} + W_{empty} \qquad [2\text{-}1]$$

Normally, the design mission gives the crew and payload weights while fuel weight and empty weight are both unknown. Using fractions of the total takeoff weight to change the fuel and empty weights for calculation. In this design, it is electric power and automatically, does not the crew and fuel, thus the equations become:

$$W_0 = W_{payload} + W_{empty} \qquad [2\text{-}2]$$

$$W_0 = \frac{W_{payload}}{1-(W_e/W_0)} \qquad [2\text{-}3]$$

Table 2-1 is the data of E-VTOL aircrafts around the world. Their fractions of the total takeoff weight is between 0.41 and 0.8, the A³ Vahana, EHang 184 and PAV-UL are between 0.41-0.67 which the number of the passage is one. Choosing the 0.6 as the fraction of the total takeoff weight, and the weight of payload is 120 kg, so the total weight is 300 kg.

Table 2-1 Data of E-VTOL Aircraft

	No. of people	W_o (kg)	W_e (kg)	$W_{payload}$ (kg)	Wing Span (m)	W_e/W_0
A³ Vahana	1.00	815	475	90	6.25	0.58
Passenger Drone	2.00	360	240	120		0.60
Aurora eVTOL	2.00	800	575	225	8.00	0.72
Avianovations Hepard	2.00	520	390	130		0.75
Bartini	4.00	1100	700	400	4.5	0.64
CarterCopter	4.00	1814	1452	363	10.40	0.80

Table 2-1—*Continued*

EHang 184	1.00	360	240	120		0.67
Lilium Jet “Eagle”	2.00	640	440	200		0.69
Skycar M400	2.00	1090	765	325		0.70
PAV-UL	1.00	330	135	195	3.50	0.41
CityHawk	4.00	1930	1170	760		0.61
Vimana	4.00	1050	650	400	10.00	0.62
Volocopter	2.00	450	300	150		0.67
TriFan 600	6.00	2404	1588	816	11.50	0.66

2.2.2 VTOL tech

The major task of VTOL technology developers is to find the design to meet hover and cruise performance, and also meet the environmental and economic requirements.

Tiltwing and ducted fan are suitable for the E-VTOL aircraft, but the one of the most efficient way is directly use the wing lift. Ullman, etc. [12] proposed a wing design, using the ducted fan to generate the flow to blow the wing top. According to Bernoulli equation, the wing will generate the vertical force that is lift. They designed and tested this ideal with the aviation aircraft and found it can almost take off vertically. This design does not need any tilt mechanism. Also Deere, etc. [13] researched on the distributed system which let the electric propellers distributed mount in front of the wing, the propellers blow the wing to increase the lift. It is good ideal to using this technology for E-VTOL.

In the jet fighter, thrust vectoring technology was used for STOL (Short Take Off and Landing)/VTOL. It uses the vectoring nozzle to change thrust direction. Figure 2-1 illustrates some vectoring nozzles; they can also apply to the electric system, like the ducted fan.

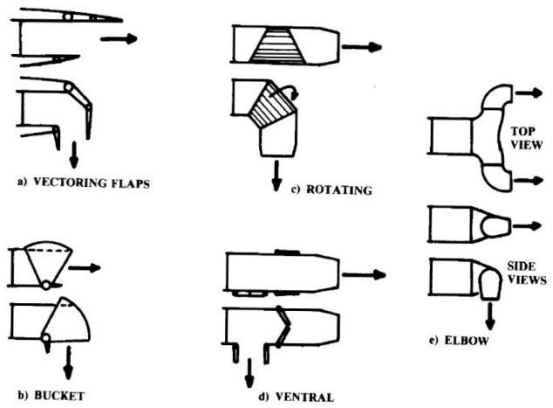

Figure 2-1 Vectoring Nozzles [14]

The presence of ducted fans change the slipstream state downstream of the propeller, reduces the slipstream velocity and slipstream energy loss, and thus converts more kinetic energy into pressure energy. So part of thrust in the case of ducted fan is produced form the propeller, the other part like the jet engine. If mounted with the contracted vectoring nozzle, it can be used for VTOL.

This design adopts both the direct lift way and ducted fan with vectoring nozzle. Figure 2-2 shows the sketch of the vertical system, the upper and lower airfoil is given by an airfoil, which means, the two airfoils are cut from the original airfoil, the contracted vectoring nozzle is also a part of the wing like flap system.

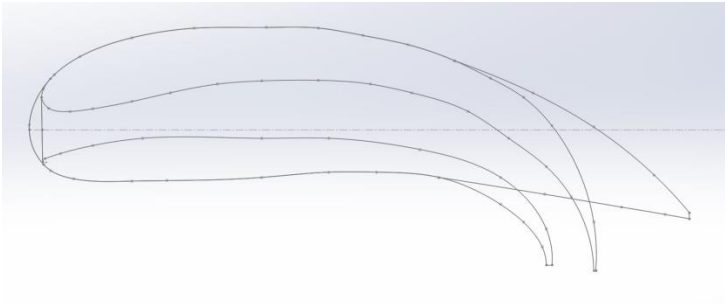

Figure 2-2 Wing Section

2.2.3 Stability

When the aircraft flies vertical, figure 2-2, the trailing edges will be flapped up, so the thrust of ducted fan changes direction to vertical, balance with the force of vertical direction which is the sum of pressure integration and viscous force (F_L), follows the principle of the lever. When aircraft flies forward, in the flight system, stability of the aircraft is that, after the slight disturbance disappears, the aircraft can automatically restore to original state without the pilot's intervention. When center of gravity is ahead of neutral point (lift point), it is stable, otherwise it is unstable. This E-VTOL's CG is behind of NP, but it is stable, as shown in the figure 2-3 , when slight disturbance happens, the lift will increase, the component of thrust also increases to generate reverse moment, so it is stable.

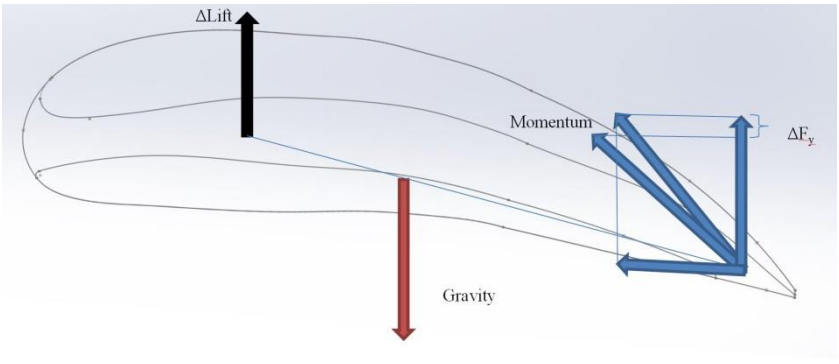

Figure 2-3 Force on Airfoil after Disturbance

2.2.4 Parameters

The purpose for this aircraft is to use it in the urban area. So the size should be limited. Compared to the car size, normally the width is around 4m, and length is less than 2.6 m. The lift is generated by wing, so the wing needs more area, and the aspect ratio needs greater to reduce the drag.

The lift force is given by $L = \frac{1}{2}\rho V^2 S C_L = W_0$, assume the C_L is 0.8.

When adopting the fly wing configuration and the wing span is 2.5 m, the chord length is about 2 m. Due to the smaller aspect ratio, mounting the plate winglet to reduce the drag and also the winglet provides function of landing gear system. Figure 2-4 is the E-VTOL aircraft model.

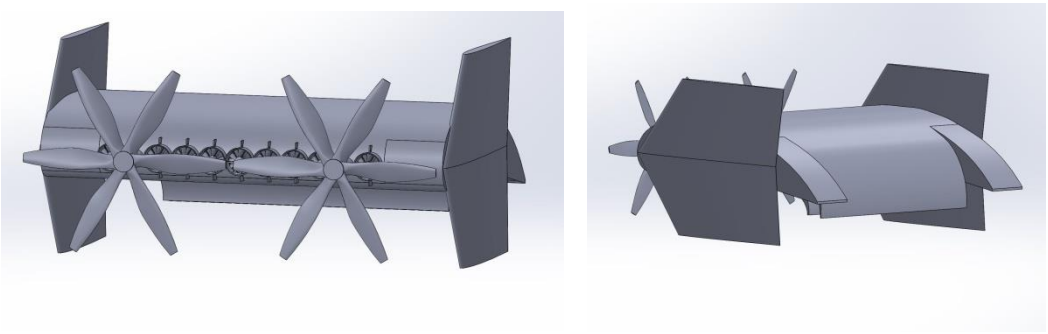

Figure 2-4 E-VTOL Aircraft

2.2.4 Objectives

From all the design details, the airfoil in the most important for this design, it can affect the lift and also the Momentum Force. When aircraft flies vertically, if the gap between the two airfoils is not clean or has shift angle that will cause the flow separate, it cannot provide enough force for vertical taking off. Also the shape that two airfoils are formed is not good, the lift performance will be not the best. So the goal of this thesis is to use the optimization design method to get the best airfoil shape for vertical situation.

Chapter 3 Aerodynamic Optimization Design

3.1 Aerodynamic Optimization Design Method

Optimization is the common problem that people solve in engineering, science and other areas. Optimization requires finding the best way among the hundreds or thousands approaches, using mathematics to find the conditions that make the objective function to be minimum or maximum.

Design Optimization finds a reasonable combination of design parameters under certain constraints to let the objective function of performance be maximum or minimum. At present, there are two kinds of approaches of aerodynamic design, Inverse Design and Direct Optimization Design [15].

Inverse design is a common method which is applied in many areas, for example, in the heat transfer problem, numerical inverse analysis is used to predict properties of heat generating material by measuring temperature at outer boundary. Accuracy and efficiency of the method is enhanced by using accurate sensitivity information by use of Semi-Analytical Complex Variable Method (CVSAM). Sensitivity information is beneficial in determining reliability of the system [16] [17] [18]. When designing the airfoil, the inverse design is to design the airfoil to get the satisfied the distribution with the given pressure distribution. In the aerodynamic optimization design, the inverse design method [19] has achieved great success, but this method has some difficult problems that cannot be solved. For example, the objective function is closely related to the design process and it is hard to give the objective pressure distribution or initial shape. These deficiencies greatly limit the widespread use of inverse design.

Compared with the traditional inverse design method, the Direct Optimization Design [20] has a greater advantage. It can not only treat the pressure distribution difference as an objective to deal with the traditional aerodynamic inverse design

problem, but also select the aerodynamic characteristics such as lift-drag ratio and drag as the objective functions, directly optimizing the characteristics. Direct Optimization Design Method is used to choose the optimization parameters and determine the geometric parameterization method of the shape, that is, design variables first. By correcting the design variables, the aerodynamic shape of the airfoil will be continuously adjusted, so the aerodynamic performance is gradually improved, and then the optimal conditions for aerodynamic performance (such as the maximum lift-to-drag ratio, minimum drag, etc.) under the constraint conditions are obtained. Direct Optimization Design combines the aerodynamic analysis and optimization theory, and realizes the automatic and robust aerodynamic design by using the high-speed computing power of modern computers, effectively improving the design ability.

Aerodynamic analysis method and optimization algorithm are the main factors that determine the design result of Directed Optimization Design. Therefore, how to choose the reasonably aerodynamic analysis methods and optimization methods (algorithms) are the most highlight issues that need to be considered. The aerodynamic analysis methods commonly used in aerodynamic optimization design are: engineering method, numerical simulation method based on potential flow theory, numerical simulation method based on Euler equation and numerical simulation method based on Navier-Stokes equation. The commonly used optimization methods are the traditional deterministic methods such as the gradient method and the penalty function method.

Among the traditional optimization methods, optimization methods based on gradient information are most widely used. The gradient method requires calculating the gradient formed by the derivative of the objective function for each design variable (sensitivity derivative). The optimization process (such as the steepest descent method, the quasi-Newton method) calculates and searches the direction in the negative direction

of the gradient, and after obtaining the minimum value in the search direction, repeats the process until the gradient is too small or the target cannot be improved. As the number of design variables increases, the cost of design optimization increases as the amount of gradient calculation increases.

In recent years, people pay more attention to design methods based on control theory. Compared with the traditional gradient method, the calculation decreases, especially when dealing with multiple design variable optimization problems, which is one of the biggest advantages of this method. The method is based on the mathematical theory controlled by the system of partial differential equations. It sets the boundary shape as control function and the flow control equation as the equality constraint, but uses the objective functional as the design target, so the design problem is transformed into a searching optimal control problem that satisfied constraints. In fact, the method directly obtains the gradient of the objective function to the design variable by establishing and solving the conjugate equation of the flow basic equation, and avoids calculating the sensitive derivative for each design variable, so it is also called the conjugate equation method. Jameson and Reuther et al. [21] [22] verified this optimized design based on the Euler equation, and the Navier-Stokes equation apply for airfoil, wing et al.

Although control theory design method has the advantage of small calculation, it is undeniable that this method only solves the problem of fast solution of gradient, it still belongs to the category of gradient method, so that global problems still remain unresolved. This is a shortcoming of most gradient-based optimization methods. If obtaining globally optimal results, the random methods such as evolutionary algorithms and modern intelligence methods must be used.

3.2 Optimization process

Optimization process can be divided into different unique modules, so that different people can change the method according to their requirements. Figure 3-1 illustrates the concept of the design optimization process.

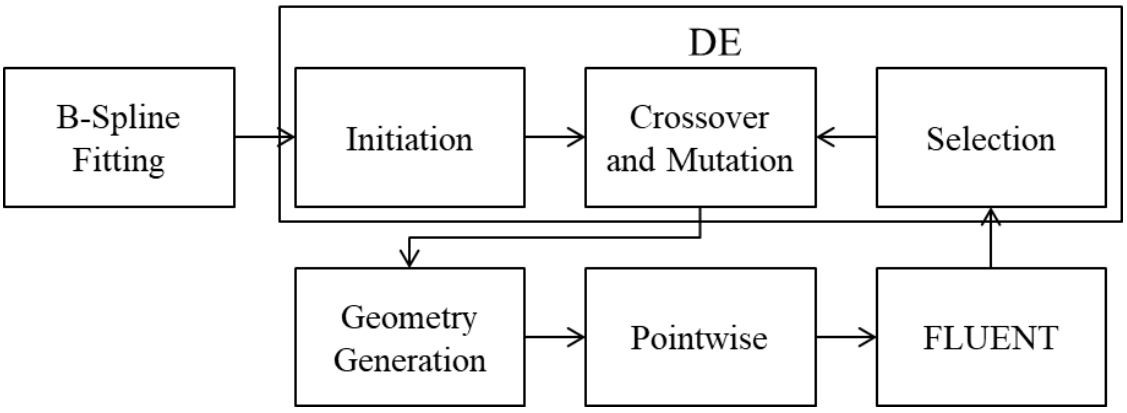

Figure 3-1 Optimization Process

First step is to get the parameters that need to be optimized by optimization algorithm geometry. Using B-spline to fit the input geometry, in this thesis is airfoil, and gets the control points. Second step is to using optimization algorithm to give the candidates. Third step is geometry generation, in this work, is airfoil, using the B-spline to give the airfoil coordinates that can be imported into mesh generation code or software. Then, mesh generation code or software like pointwise generates the mesh and output the mesh or case file. Next, the CFD solver, it could be software like FLUENT, OpenFOAM or CFD code to simulate the flow, and write the results to post processing. In this work, the post processing is to calculate the total force, which is the sum of F_L and momentum force. At last the optimization algorithm will compare and choose the best result. Every step will be explained in detail in the following chapters.

The optimization process needs less intervention of user, the whole process should be automated. The current optimization process adopts following software: FLUENT and Pointwise. These software normally need user to operate, which is not

good for optimization, and thus individual module needs script files to reduce the intervention. A script contains a list of commands; the system can read it and translate it into operation. The software can work automatically after reading the script. Different software has its own script language, so the hard work is to program different scripts. Also to make the optimization process automatically, it needs the shell script to call for each part.

Chapter 4 Optimization Toolboxes

4.1 B-spline

The B in B-spline is basic, which means it the general spline. B-spline is piecewise polynomials spline, developed from Bezier. It modified the disadvantages of the Bezier. In the Bezier, every point is controlled by the whole control points, so if changing one control point would change the whole curve. But B-spline can change local curve without effect on other parts. Also, the order of B-spline is not controlled by the number of the control points.

4.1.1 Recursion Formula

B-splines use the recursion formula to generate the parametric curves. A set of defined polygon points express the spline. Its dimensions directly determine the dimensions of spline. If n+1 is the control points, k is the order, the B-spline consists of (n+1)-k segments. The formulas that define B-spline are[23]:

$$X(u) = \sum_{i=1}^{n+1} B_i \times N_{i,k}(u) \qquad [4\text{-}1]$$

$$N_{i,j}(t) = \begin{cases} 1 & if \quad x_i \le t < x_{i+1} \\ 0 & otherwise \end{cases} \qquad [4\text{-}2]$$

$$N_{i,j}(t) = \frac{(u - x_i) \times N_{i,k-1}}{(x_{i+k-1} - x_i)} + \frac{(x_{i+j} - u) \times N_{i+1,k-1}}{(x_{i+k} - x_{i+1})} \qquad [4\text{-}3]$$

In the equations, $B = [B_x \ B_y \ B_z]$, represent the control points' coordinates. $X(u) = [x(u) \ y(u) \ z(u)]$, represent the curve coordinates. $N_{i,j}(t)$ are the node vectors.

4.1.2 Fitting Method

In the optimization process, it needs using B-spline program twice, at the first and third steps. At the first to fit the airfoil, which gives the control points and at the third step to give the airfoil coordinates by control points. Matrix form is easy to program for computer to solve the problem, so changing the equations into the matrix form gives:

$$[N][B]=[X] \quad \text{[4-4]}$$

where $[N]$ is the shape factor matrix or node vector matrix; $[B]$ is the control point matrix; $[X]$ is the curve coordinate matrix.

Airfoil data is easy to get by using this matrix and it also can be used for fitting. When fitting the curve, the X matrix is known, B matrix is unknown, but to some degree, the N matrix is also unknown. The ideal is to assume intervals, so that the N matrix must be generated. Choosing the different intervals can cause different results.

Really, this is just a case of solving a set of simultaneous equations. However, at this point, it will require the number of the input data to be equal to the control point's number but it not practical, because the control points are much less than the inputs. Therefore, it is necessary to convert matrix equation, multiplying transpose of N both side [24], so the result is

$$[N]^T[N][B]=[N]^T[X] \quad \text{[4-5]}$$

Because it needs to get the B matrix, the inversion should be applied, the equation can be written as:

$$[B]=\{[N]^T[N]\}^{-1}[N]^T[X] \quad \text{[4-6]}$$

This method is the direct method, only has rounding errors, not like the approximation curve fitting methods that have the approximation error. This method is highly reliable and accurate [24].

4.1.3 Fitting results

In this work, the B-spline is used to fit the two airfoils. When testing the codes, the k= 4 and n=34 is used as it has less rounding error. The fitting result is shown in the figure 4-1. Figure 4-2 shows all the control points, the points between the lines are chosen for optimizing. The reasons to choose these points are as follows: First, the airfoils should be at the same relative positions so the leading and trailing edge should be kept at the same place and second, changing these points can cause much effect on camber of the unit-airfoil which has impact on the lift. Last, the shift turning place will cause the flow separation, choosing this section as it has the shift turn.

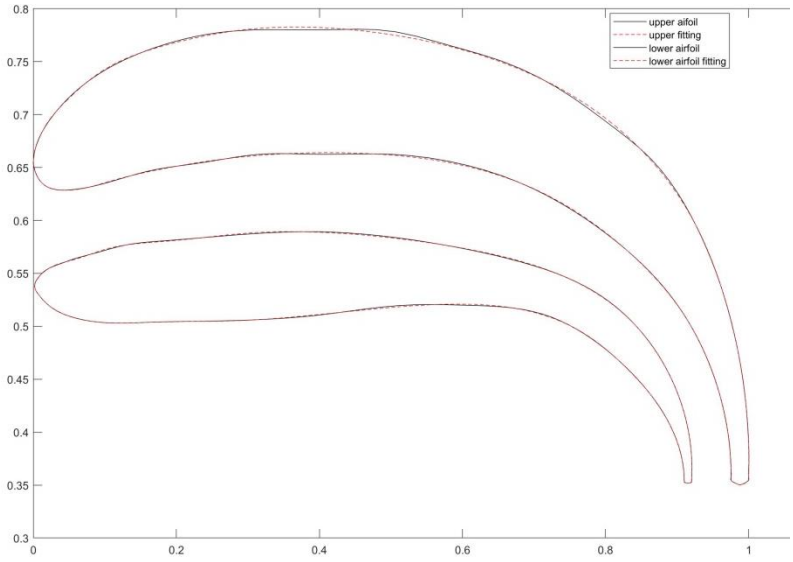

Figure 4-1Fitting Airfoil

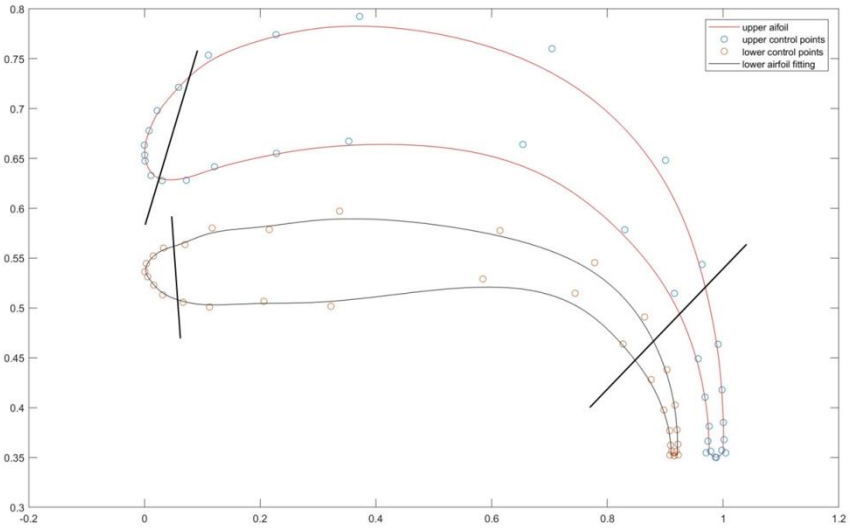

Figure 4-2 Control Points

4.2 Meshing

In computational fluid dynamics, grid is the collection of discrete points distributed in a flow field according to a certain rule. The process of distributing these mesh nodes is called Grid Generation. Grid generation is critical to CFD and is directly related to the success or failure of CFD calculations.

4.2.1 Structured grid

Structured grid contains only quadrilaterals or hexahedrons which were original grid for using CFD analysis of aeronautical areas between 1970s and 1980s [25]. During that time finite difference method dominated the CFD technology, so it is natural to choose the structured grid to discrete the geometry. If writing a CFD code, using structured grid ,it is very easy to get the value from the neighbors, for example, figure 4-3 is the 2D structured grid of finite difference method, by using this grid, the derivative of $u_{i,j}$ can be obtain from $u_{i+1,j}$, $u_{i-1,j}$ so it has many coding advantages. Structured grid also provides accurate solutions to flow problem, and it needs less memory. Because the

structured grid is the uniform mesh, the number of nodes on each layer needs to be equal. So it is difficult to generate the mesh with the complex shape.

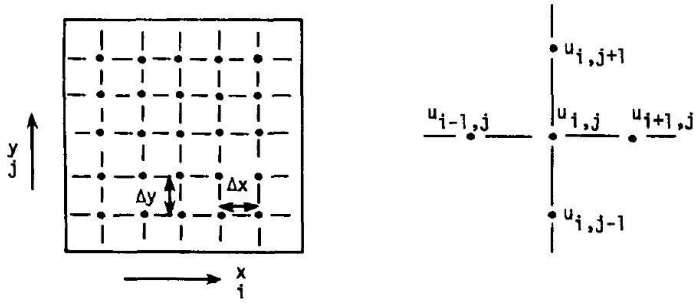

Figure 4-3 2D Structured Grid [26]

$$\frac{\partial u_{ij}}{\partial x} = \frac{u_{i,j} - u_{i-1,j}}{\Delta x} + \mathrm{O}[(\Delta x)] \quad [4\text{-}7]$$

$$\frac{\partial u_{ij}}{\partial x} = \frac{u_{i+1,j} - u_{i-1,j}}{2\Delta x} + \mathrm{O}[(\Delta x)^2] \quad [4\text{-}8]$$

4.2.2 Unstructured grid

In the late 1980s, unstructured grid was widely applied to computational aeronautics [27]. Unstructured grid method utilizes the flexibility of triangular (two-dimensional) or tetrahedral (three-dimensional) in defining complex shapes, using them to fill the two-dimensional (three-dimensional) space based on Delaunay method or wave front method. Unstructured grid eliminates the nodes' constraints of structured grid, makes the nodes and cells have good controllability, so it can deal with the boundaries better, and is suitable for simulating real flow of the complex shapes. Unstructured grid uses a certain criterion to optimize and judge during its generation process, so it can generate high-quality meshes and is easy to control the size of the mesh and the density of nodes. Random data structure is adopted that is a benefit for grid adaptation. Once the distribution of the mesh is specified on the boundary, the mesh can be automatically

generated between the boundaries without the need for blocks or user intervention, and there is no need of information transformation between the subdomains. Therefore, in recent years, the unstructured grid method has received a high degree of attention and has been greatly developed.

The main disadvantage of the unstructured grid is that it cannot deal well with the viscous problem. Only triangle or tetrahedral meshes are used in the boundary layer lead to extremely large number of grids. However, now the hybrid mesh technique is the better method to solve this problem. Figure 4-4 is the hybrid mesh, it generates a quadrilateral or triangular prism mesh that can be used for viscous calculations on the boundary layer, and then generate a triangular unstructured grid from the quadrilateral or triangular prism mesh's boundary.

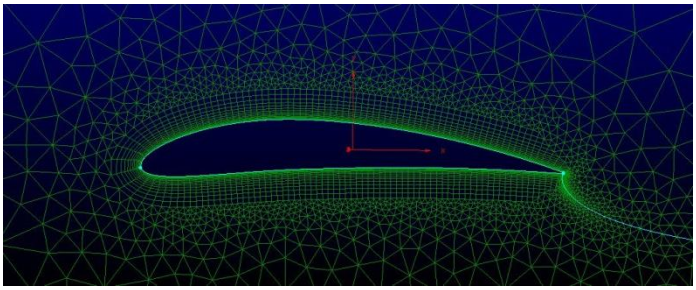

Figure 4-4 Hybrid Mesh

4.2.3 Mesh consideration

The computational accuracy of unstructured and structured grids is mainly due to the quality of the mesh (orthogonality, aspect ratio, etc.) and the algorithms, not to the topology (either structured or unstructured), also the differences in their respective advantages are becoming less and less obvious. A Baker [28] tested different kinds of mesh. Although, the multiblock structured grid is the highest viscous accuracy, it still suggests that a hybrid mesh is the best for automation and optimization process by balance the accuracy and time cost. For this work, it is an optimization problem, it will

generate a lot of meshes. Considering the computational time required, without compromising the accuracy, hybrid mesh is used.

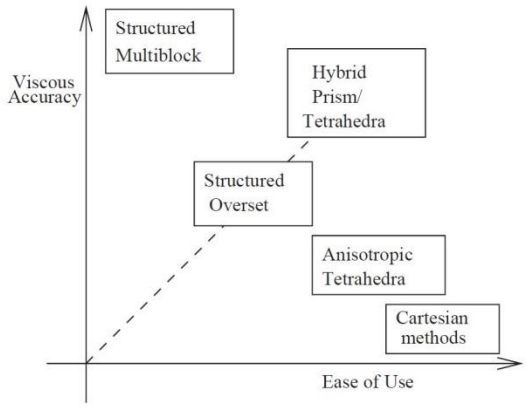

Figure 4-5 Accuracy of Different Mesh Types [28]

4.2.4 Pointwise

Pointwise is the grid software which developed from Gridgen. It has a good advanced and automated algorithm, T-Rex, to generate the hybrid mesh for a complex geometry. T-Rex algorithm extrudes layers and optimizes cell quality to get the high-quality hybrid meshes. First, it distributes points around the surface mesh' perimeter after the algorithm starts. Then extruding (or advancing) the boundary points into the surface grid. During the extruding, collision test is also processing to make sure the candidate does not collide with any other extrusion front. When extruded triangle is isotropic, or Max Layers is reached, extrusion will stop [29].

Pointwise V18.02 was used in this thesis. The whole process is automated, so the grid generation does not need user to operate. The Pointwise script can generate grid automatically. Glyph2 is the language for the writing the script, based on Tcl. In the Glyph2, operations start from pw::Application that is the one of the global types [30]. Usually, it uses 'pw::<typename>' command to begin, for example, the 'pw::Application setCAESolver "ANSYS FLUENT" 2' is to choose the FLUENT solver. In Pointwise, it

uses Database to express the CAD model; connector to express the line mesh, 1D; domain to express face mesh, 2D; block to express volume mesh, 3D. To automatically generate the mesh, in the script file, it should have code to import the airfoil X Y data, generate the database and then connectors, domains and apply to T-Rex step by step.

4.3 CFD

4.3.1 Discretization Methods

With the development of computer technology and computational methods, many complex engineering problems are solved by CFD. Numerical simulation depends on discretization methods. The grid is the basis of discreteness, and the grid nodes are the storage locations of discretized physical information. There are three discretization methods, finite difference method, finite element method and finite volume method.

The finite difference method (FDM) is the most classical method in numerical simulation. It divides the computational domain into a differential mesh, which is used to replace the continuous solution domain. It replaces the partial differential equation with difference quotient to derive difference equations in the discrete points. The method is more used to solve hyperbolic and parabolic problems. There are many ways to construct the difference, at present, the Taylor series expansion method is mainly used. There are four basic forms of differential expression: first-order forward difference, first-order backward difference, first-order center difference, and second-order center difference [26]. The first two are first-order, and the last two are second order. Different combinations of time and space can be combined into different differential calculation formats. FDM can get the higher accuracy, and it is easy to program and easy to parallel. But it not suitable for to complex mesh, due to it requires continuity of the area.

The finite element method (FEM) divides the continuous computational area into a number of small elements randomly and constructs an interpolation function in each

small element, and then transforms the control equation problem into finite element equations of all elements according to the extremum principle (variation or weighted residual method). At last, to assemble all the local elements, so the solution of computational area is the sum of the extremum of each element. It has better adaptability to elliptical problems. The finite element method is slower than the FDM and FVM, so it is not widely used in commercial CFD software.

The finite volume method (FVM) is also called control volume method. It divides the calculation area with meshes, and there is an unrepeated control volume around each grid point, so it integrates the differential equation with each control volume to get the set of discrete equations. The unknown valves are the variable on the mesh node. The subdomain method plus discretization is the basic idea of the finite volume method. Finite volume method is easy to understand and has the physical meaning based on the conservation principle. The discrete equations obtained by the finite volume method require that the integral conservation of the variable is satisfied for any control groups which is the advantage of the finite volume method. Finite Volume Method is suitable for fluid calculations, can be applied to complex grids, it is suitable for parallelism. But the accuracy can only be second order.

4.3.2 Numerical method

Navier-Stokes (NS) equations are solved in traditional computational fluid dynamics. According to the different processing scales of the turbulence in the NS equation, the turbulent numerical simulation methods are mainly divided into three types: direct numerical simulation (DNS), large eddy simulation (LES) and Reynolds average approach (RANS). Direct numerical simulation (DNS) is used to directly calculate the three-dimensional unsteady N - S equations without any turbulence model, and calculate the time evolution of all instantaneous motions, including pulsation, of turbulence in the

three-dimensional flow field to obtain accurate information on the turbulent flow. It is an effective way to study the turbulence mechanism. The main disadvantage of DNS is that it requires a very large computer memory and consumes a lot of time.

The large eddy simulation is based on the turbulent kinetic energy transfer mechanism, which directly calculates the motion of large-scale vortices, but the effect of small eddy vortex motion on large eddies is calculated by modeling. So it can obtain more dynamic information, like large-scale vortex structures, more than the Reynolds averaging method, and saves time of simulation compared with direct numerical simulation. Since the actual turbulence is extremely complicated, it still requires a very considerable calculation time and requires large computer storage capabilities.

The Reynolds average approach (RANS) applies the turbulent statistical theory to simulation to solve the unsteady N-S equations over average time. The so-called turbulence model theory is based on the theoretical knowledge of turbulence, experimental data or direct numerical simulation results, making various assumptions about Reynolds stress. The requirements for the computer are low, and the calculation results can be obtained which can meet the engineering requirements. It is possible to solve almost all engineering problems with different the Reynolds number. However, RANS just gives the average results, and the detailed information of the turbulence flow cannot be given. Also it relies on boundary conditions of the flow field and experience.

In this thesis, Reynolds average approach (RANS) is used due to the time consumption, computer memory and the results of turbulence flow is accuracy enough for this problem.

4.3.3 Continuity equation

In the microscopic scale, the physical properties of individual molecules are violently non-uniform, but in macroscopic field, the scale of molecules is much less than

the aircraft characteristic length and hence the fluid can be considered continuity. There is a control volume V, its surface is S. The decrease in rate of mass inside is the volume mass differential, so the

$$\Delta mass = -\frac{d}{dt}\int_V \rho dV = \int_V \frac{\partial \rho}{\partial t} dV \qquad [4\text{-}9]$$

On the other hand, the fluid will flux out, so the

$$\Delta out = -\int_V \rho \vec{v} dS = \int_V \nabla \cdot \left(\rho \vec{v}\right) dV \qquad [4\text{-}10]$$

where $\nabla \cdot \left(\rho \vec{v}\right) = \frac{\partial(\rho u)}{\partial x} + \frac{\partial(\rho v)}{\partial y} + \frac{\partial(\rho w)}{\partial z}$.

The mass of the volume is conserved, so the decrease rate of mass should equal with mass flux out's rate, which is the continuity equation [31]:

$$\frac{\partial \rho}{\partial t} + \nabla \cdot \left(\rho \vec{v}\right) = 0 \qquad [4\text{-}11]$$

Now introducing the material (or substantive) derivative [31]

$$\begin{aligned} \frac{D\rho}{Dt} &= \frac{d}{dt}\rho(x(t), y(t), z(t), t) \\ &= \frac{\partial \rho}{\partial t} + \frac{dx}{dt}\frac{\partial \rho}{\partial x} + \frac{dy}{dt}\frac{\partial \rho}{\partial y} + \frac{dz}{dt}\frac{\partial \rho}{\partial z} \\ &= \frac{\partial \rho}{\partial t} + u\frac{\partial \rho}{\partial x} + v\frac{\partial \rho}{\partial y} + w\frac{\partial \rho}{\partial z} \\ &= \frac{\partial \rho}{\partial t} + \vec{v} \cdot \nabla \rho \end{aligned} \qquad [4\text{-}12]$$

So continuity equation can be written is this form:

$$\frac{D\rho}{Dt} + \vec{v} \cdot \nabla \rho = 0 \qquad [4\text{-}13]$$

In this study, the E-VTOL flies under the low speed condition, so the fluid is incompressible, $D\rho/Dt = 0$, so the continuity equation can be reduced as

$$\nabla \cdot \vec{v} = 0 \ or \ \frac{\partial u}{\partial x} + \frac{\partial v}{\partial y} + \frac{\partial w}{\partial z} = 0 \quad [4\text{-}14]$$

4.3.4 Momentum equation

There is a control volume V, its surface is S. The momentum change inside is

$$momentum\ change = \frac{d}{dt}\int_V \rho \vec{v} dV = \int_V \rho \frac{D\vec{v}}{Dt} dV \quad [4\text{-}15]$$

There are two forces, body and surface force, act on the volume inside and surface respectively. So the total force change is

$$Total\ change\ \ force = \int_V \rho \vec{v} dV + \int_S -p\hat{n} dA = \int_V (\rho \vec{g} + \nabla \cdot (-p\hat{n})) dV \quad [4\text{-}16]$$

The momentum is also following the law of the conservation, so [32]

$$\rho \frac{D\vec{v}}{Dt} = \rho \vec{g} + \nabla \cdot (-p\hat{n}) \quad [4\text{-}17]$$

In Cartesian coordinates, it can be written x, y, z momentum [32],

$$\frac{\partial \rho u}{\partial t} + \frac{\partial (\rho u^2)}{\partial x} + \frac{\partial (\rho uv)}{\partial y} + \frac{\partial (\rho uw)}{\partial z} = -\frac{\partial p}{\partial x} + \nu \nabla^2 u$$

$$\frac{\partial \rho v}{\partial t} + \frac{\partial (\rho uv)}{\partial x} + \frac{\partial (\rho v^2)}{\partial y} + \frac{\partial (\rho uw)}{\partial z} = -\frac{\partial p}{\partial y} + \nu \nabla^2 v \quad [4\text{-}18]$$

$$\frac{\partial \rho w}{\partial t} + \frac{\partial (\rho uw)}{\partial x} + \frac{\partial (\rho vw)}{\partial y} + \frac{\partial (\rho w^2)}{\partial z} = -\frac{\partial p}{\partial z} + \nu \nabla^2 w$$

4.2.5 Fluent

Reynolds averaging is used to decompose Navier-Stokes into mean components. For pressure, energy, or other scalars, the components [33]:

$$\phi = \bar{\phi} + \phi' \quad [4\text{-}19]$$

And for the velocity components:

$$u_i = \overline{u_i} + u_i' \quad [4\text{-}20]$$

The continuity and momentum equations can be written as [33]:

$$\frac{\partial \rho}{\partial t} + \frac{\partial}{\partial x_i}(\rho u_i) = 0 \quad [4\text{-}21]$$

$$\frac{\partial \rho}{\partial t}(\rho u_i) + \frac{\partial (\rho u_i u_j)}{\partial x_j} = -\frac{\partial p}{\partial x_i} + \frac{\partial}{\partial x_j}\left[\mu\left(\frac{\partial u_i}{\partial x_j} + \frac{\partial u_j}{\partial x_i} - \frac{2}{3}\delta_{ij}\frac{\partial u_l}{\partial x_l}\right)\right] + \frac{\partial}{\partial x_j}\left(-\rho\overline{u_i' u_j'}\right) \quad [4\text{-}22]$$

They are called Reynolds-averaged Navier-Stokes (RANS) equations. Compared with Navier-Stokes equations, the new equations lead to Reynolds stress term, that captures the effects of turbulence. To close the equations above, different turbulence models were developed to approximate the Reynolds stress term.

Spalart-Allmaras model is a one-equation model, which directly solves the modified turbulent viscosity for the aerospace field with bounded wall flow [34]. This model can also be used for coarse meshes. The time cost of calculation is less, and it can give the good results for a certain complicated boundary layer problem, especially for the flow around surface, but the calculation result is not widely tested, and the sub-model is lacking.

Standard $k-\varepsilon$ model is the two-equation model that is the default $k-\varepsilon$ model in FLUENT and its coefficients are given by empirical formulas. Standard $k-\varepsilon$ model is suitable only for the turbulence in high Re number. This model is widely used in engineering area, due to its convergence and calculation accuracy can meet general engineering calculation requirements. However, it cannot give the good results when it

applies for the complex flow simulation effects such as large curvature and strong pressure gradient, and also not suitable for simulating swirl and flow.

RNG $k-\varepsilon$ model is the deformation of the Standard $k-\varepsilon$ model, the equations and coefficients are derived from the analytical solution. It added a new condition in ε equation to improve the accuracy. It can use to predict medium intensity vortex and low Reynolds number's flow. It can simulate medium-complex flows such as jet impact, separation flow, secondary flow and swirl. It is limited by the vortex viscous assumption, so it cannot simulate for the strong swirl.

Realizable $k-\varepsilon$ model is also the deformation of the Standard $k-\varepsilon$ model. It uses mathematical constraints to improve the performance of the model. The performance of the Realizable $k-\varepsilon$ is same as the RNG $k-\varepsilon$ model.

Standard $k-\omega$, in this model, k and ω are solved by two transport equations. It has better performance for the bounded wall surface and low Reynolds number's flow, especially the problem of the flow around surface. It is suitable for boundary layer flow with a reverse pressure gradient, separation and transition flow.

SST $k-\omega$ model is deformation of Standard $k-\omega$. It used a blending function to combine the Standard $k-\varepsilon$ model with the $k-\omega$ model. Basically it is the same as the Standard $k-\omega$ model. It is not suitable for free shear flow due to strong dependence of wall distance.

Reynolds Stress model, it directly uses the transport equation to solve the Reynolds stress, avoiding the viscous assumptions of other models. It has strong advantages over other models at simulating strong swirl flow. It is the most complex RANS model, so it takes up more CPU time and memory, convergence is also difficult. It is suitable for complex 3D flow.

The work of this thesis is to simulate the airfoil, it is the flow around surface problem, and also optimization needs the time of every flow simulation to be less. Thus, the S-A model was chosen.

The Spalart-Allmaras model is also called a low-Reynolds number model, due to it is effectively model in low Re number. It requires the boundary layer to be properly resolved (y^+) that is in the viscosity-affected region. In FLUENT, the Spalart-Allmaras model allows the model independent of the near wall y^+ resolution's application, by extending with a y^+ insensitive wall treatment [33].

Because Spalart-Allmaras model does not calculate the k , so the Reynolds stresses can be reduced, so the [33]

$$-\rho\overline{u_i'u_j'} = \mu_t\left(\frac{\partial u_i}{\partial x_j}+\frac{\partial u_j}{\partial x_i}\right) \quad \text{[4-23]}$$

In the Spalart-Allmaras model, the transported variable, $\tilde{\nu}$ is the turbulent kinematic viscosity except in the near-wall, the transport equation of S-A is [34]

$$\frac{\partial}{\partial t}(\rho\tilde{\nu})+\frac{\partial}{\partial x_i}(\rho\tilde{\nu}u_i)=G_\nu+\frac{1}{\sigma_{\tilde{\nu}}}\left\{\frac{\partial}{\partial x_j}\left[\left(\mu+\rho\tilde{\nu}\right)\frac{\partial\tilde{\nu}}{\partial x_j}\right]+C_{b2\rho}\left[\frac{\partial\tilde{\nu}}{\partial x_j}\right]^2\right\}-Y_\nu+S_{\tilde{\nu}} \quad \text{[4-24]}$$

where Y_ν is the destruction of turbulent viscosity, the production of turbulent viscosity is G_ν . $C_{b2\rho}$ and $\sigma_{\tilde{\nu}}$ are the constants. $S_{\tilde{\nu}}$ is a user-defined source term. The molecular kinematic viscosity is ν [33].

FLUENT v18.2 is the one of widely used commercial CFD software that is based on FVM discretization method. Because this case is the low speed condition, choose the pressure-based solver which is suitable for incompressible flow. There are two algorithms for pressure-based solver, the segregated algorithm was chosen. The segregated

algorithm is more memory efficient than coupled algorithm, due to storing the discretized equations in the memory one at a time, although the solution convergence is slower than coupled algorithm. In segregated algorithm, pressure-velocity coupling is used to derive an additional condition for pressure. There are five pressure-velocity coupling algorithms: SIMPLE, SIMPLEC, PISO, Coupled, and Fractional Step (FSM) [33]. SIMPLE was chosen that is good for convergence and high mesh skewness [35].

Propeller and fan are different to simulate, there still is not accurate theory, momentum theory, blade element theory and vortex theory are applied now. To simplify the simulation, using the momentum theory, it ignores the blade effect [36] [37], so in the boundary condition, setting the fan and propeller as the velocity-inlet.

For the Spatial discretization, the node-based gradient was chosen, which is more accurate than the cell-based gradient especially for unstructured grids, although, it is relatively more expensive to compute. And the second-order was chosen for pressure, momentum and turbulent viscosity. For unstructured meshes, using the second-order discretization can get the more accurate results, especially for complex flows. A multidimensional linear reconstruction approach was used to compute quantities at cell faces to preserve the second-order accuracy. A Taylor series expansion of the cell-centered solution is used in this approach [33].

Initialization is used to calculate the initial value of flow field, including pressure, velocity, temperature and turbulence coefficient. In theory, the given initial field will not affect the final result, because with the increase in the number of iterations, the calculated flow field will approximate to the real flow field. However, due to the FLUENT has the discretization error and truncation error, if the initial field is much deviation from the actual physical field, it will be difficult to obtain convergence, or could even diverge at the beginning of the iteration. In the new version, the FLUENT has the Hybrid

Initialization that is a boundary interpolation and collection of recipe methods. The velocity field and the pressure field that conforms to complex domain geometries are produced by solving the Laplace equation in the computational domain, and according to a predetermined recipe or domain averaged values to patch the other variables [33].

All the settings were written as Text User Interface (TUI) in the script. And the data was written to the txt file that the post processing code can read.

4 Post processing

There are two force that consist the total vertical force, sum of pressure integration and viscous force (F_L), and the momentum force of vertical direction (M_y) due to ducted fan.

The actuator disk theory is also the momentum theory, which ignores the propellers [37]. Therefore, the momentum theory is used to calculate the vertical thrust. Choosing the gap area as the control volume, the inlet is the section 1, the connection of the two airfoils' trailing edge is section 2. The change in momentum during the time of dt is

$$\sum d\vec{M} = \int_{A_2} \rho dQ\vec{u}_2 dt - \int_{A_1} \rho dQ\vec{u}_1 dt \quad [4\text{-}25]$$

To simplified problem set the average velocities in the two cross section area to get the approximate solution, so the equation is

$$\sum d\vec{M} = \rho Q(\beta_2\vec{V}_2 - \beta_1\vec{V}_1)dt \quad [4\text{-}26]$$

where β_2 and β_1 are momentum correction coefficients, in engineering area, the valve is 1. So the force is

$$\sum \vec{F} = \sum \frac{d\vec{M}}{dt} = \rho Q(\vec{V}_2 - \vec{V}_1) \quad [4\text{-}27]$$

Because the velocity of vertical direction in section 1 is 0, the momentum force is $M_y = \rho Q \bar{v}_2$

Another force is sum of pressure integration and viscous force of y direction, using the F_L to express:

$$F_L = \int_0^x (P_{lower} - P_{upper}) d(x/c) + viscous\ force \quad [4\text{-}28]$$

The total vertical force is the sum of pressure integration and momentum force, $F = F_L + M_y$. The FLUENT can directly F_L report .

4.3 Optimization Algorithm

Genetic algorithm (GA), is a classical evolutionary algorithm. It became a hot research field since Holland [38] introduced in 1973. Many research efforts have been done on GA, and various improved algorithms have been proposed to improve the convergence speed and accuracy of the algorithm. Firstly, the classical genetic algorithm encodes the parameters to generate a certain number of individuals that are the initial population. Each of these individuals can be a one-dimensional or multi-dimensional vector, represented by a string of binary numbers, called a chromosome. Each binary number of a chromosome is called a gene. As the nature environment, it also meets the rule of survival of the fittest. In the algorithm, every population needs to judge by a criterion that is decided by fitness function. The individuals with good performance are selected as the parents to participate in the subsequent genetic operations to generate new generation of population, then compare, select and hybridize until the requirement is met.

The differential evolution algorithm is another evolutionary algorithm. It has become an important branch of the evolutionary algorithm (EA). Many scholars have begun to study the DE algorithm and have achieved a lot of results.

Compared with the GA, DE has some advantages. First, GA uses binary to code, and DE uses real number to code. Since binary coding is obtained by real number transformation, the probability of local convergence of GA algorithm is increased. Due to the defect of binary coding, in GA it is difficult to get real number converge solution. But DE does not need to transform, it easy to achieve the global convergence. Second, the different parameter settings of the GA algorithm have a greater impact on the final result. Therefore, in actual use, it is necessary to try different settings which increase the difficulty of using. Different from GA, the DE algorithm has two main parameters to adjust, and the parameter settings have less obvious impact on the results, so it is easier to use. Last, in the high-dimensional problem, Converting real numbers into binary processes increases the length of chromosomes. Therefore, GA converges slowly or not converge at all. However, the DE algorithm converges quickly and the results are accurate.

4.3.1 DE

The differential evolution algorithm is a random heuristic search algorithm that simulates the evolutionary development law of the natural biological population with the principle of “survival of the fittest and survival of the fittest”. In 1995, Rainer Storn and Kenneth Price [39] first time to introduce this new heuristic algorithm for minimizing optimum problem. The differential evolution algorithm has been successful applied in many areas due to its ease of use, robustness, and powerful global search capabilities.

The basic idea of the differential evolution algorithm is to start from a randomly generated initial group, and then generate a new individual by weighting the vector difference of any two individuals in the population and summing it with a third individual according to a certain rule, and then comparing the new individual with a pre-determined individual in a contemporary population, if the fitness value of the new individual is better than the fitness value of the compared individual, then the old individual is replaced by a

new individual in the next generation, otherwise the old individual remains. Through continuous iterative operations, retain good individuals, eliminate inferior individuals, and guide the search process to the optimal solution.

The differential evolution algorithm has some main advantages compared with the traditional optimization method in the design optimization. First, the differential evolution algorithm starts search from a group rather than a point, which is the main reason why it much probability can find the overall optimal solution. Second, the evolutionary criteria of the differential evolution algorithm are based on adaptive information, without the using other auxiliary information, such as the function must be differential or continuous, which greatly expands its application areas. Third, differential evolution algorithm has inherent parallelism, which makes it very suitable for large-scale parallel distributed processing, reducing time cost. Last, the differential evolution algorithm uses probability transfer rules and does not require deterministic rules.

4.3.1 Generate initial population

The first stage involves generating NP individuals randomly which meet the constraints in the dim dimensions where dim is the number of active function variables and NP is the population size. In this study there are 35 control points, but only 14 were chosen to be changed, so the dim is 14. The implementation measures are as follows:

$$x_{ij} = rand(0,1)(x_{ij}^{U} - x_{ij}^{L}) + x_{ij}^{L} \quad [4\text{-}29]$$

$$x_{ij} = rand(0,1)(x_{ij}^{U} - x_{ij}^{L}) + x_{ij}^{L} \quad [4\text{-}30]$$

$$i = 1,2,\mathrm{L}\ ,\dim; \qquad j = 1,2,\mathrm{L}\ ,NP \quad [4\text{-}31]$$

Where x_{ij}^{U} , x_{ij}^{L} are the upper and lower bounds of the jth chromosome respectively, and $rand(0,1)$ is a random fraction between [0, 1], n is the iteration number.

4.3.2 Mutation

The differential evolution algorithm corrects the values of individual population by difference vector information, so the good individuals can be preserved in evolution. The most important operation is the mutation process. Selecting three individuals x_a, x_b, x_b from the population and ($i \neq a \neq b \neq c$), so

$$y_{ij}^{n+1} = x_{aj}^{n} + F \bullet (x_{bj}^{n} - x_{cj}^{n}) \quad [4\text{-}32]$$

where $x_{bj} - x_{cj}$ is the difference vector, this differential operation is the key to differential evolution algorithms; F is the scaling factor. Figure illustrates how the vectors are generated by mutation.

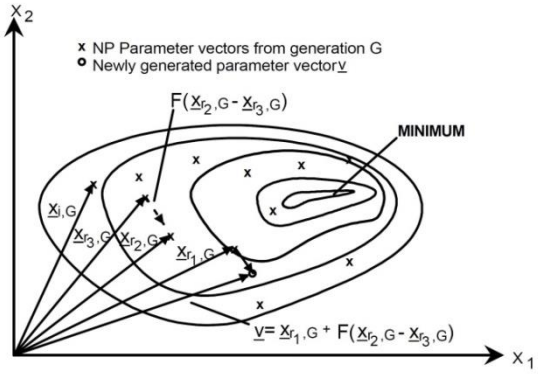

Figure 4-6 Mutant Vectors Generation [39]

Beside the standard differential evolution algorithm, Rainer Storn and Kennrth Price [40] have also proposed some extension modes for mutating operations. Here are some of the main modes:

$DE / rand / 1 / bin$

$$y_{ij}^{n+1} = x_{aj}^{n} + F \bullet (x_{bj}^{n} - x_{cj}^{n}) \quad [4\text{-}33]$$

$DE / rand / 2 / bin$

$$y_{ij}^{n+1} = x_{aj}^{n} + F \bullet (x_{bj}^{n} - x_{cj}^{n} + x_{dj}^{n} - x_{ej}^{n}) \quad [4\text{-}34]$$

$DE/best/1/bin$

$$y_{ij}^{n+1} = x_{bestj}^{n} + F \bullet (x_{bj}^{n} - x_{cj}^{n}) \quad [4\text{-}35]$$

$DE/best/2/bin$

$$y_{ij}^{n+1} = x_{bestj}^{n} + F \bullet (x_{bj}^{n} - x_{cj}^{n} + x_{dj}^{n} - x_{ej}^{n}) \quad [4\text{-}36]$$

where x_{best} is the best individual of the n th iteration; a, b, c, d, e are the random integer which indicate the individual's sequence number in the population.

Price K. V. [41] tested a large number of functional with these algorithms, and found that the results of these different DE algorithms are certainly different. Among these algorithms, the results of $DE/rand/1/bin$ and $DE/best/1/bin$ are the best. Although $DE/best/1/bin$ can accelerate convergence, it is easy to premature. This thesis uses the $DE/rand/1/bin$, because it is simple to implement.

4.3.3 Crossover

Crossover is to increase the diversity of the population, using the following function to crossover:

$$v_{ij}^{n+1} = \begin{cases} y_{ij}^{n}, \ rand\ m_{ij} \le CR \ or \ \ j = rand(i) \\ x_{ij}^{n}, \ rand\ m_{ij} > CR \ or \ \ j \ne rand(i) \end{cases} \quad [4\text{-}37]$$

where $rand\ m_{ij}$ is a random fraction between 0 and 1, CR is the crossover probability, it is great than 0, less than 1, $rand(i)$ is a random integer between 1 and n. Figure illustrates the vectors' generation, this crossover strategy ensures that x_i^{n+1} has at least one component with a corresponding component of x_i^{n}.

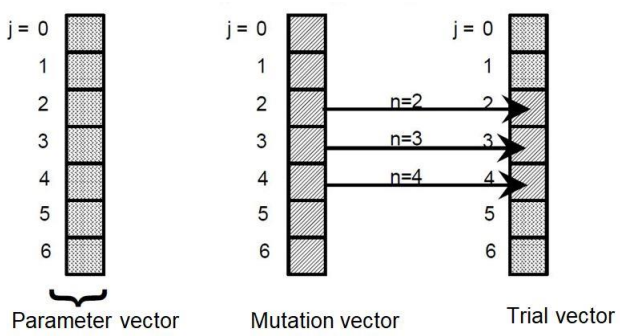

Figure 4-7 Trail Vectors Generation [39]

4.3.4 Constraint

After mutation and crossover, the airfoil may out of the limitation, so there is a setting to constraint the airfoil. Figure 4-8 is the lower airfoil example, each control point will compare with the upper and lower limitation, if out of the box, the point will change to the maximum or minimum limitation.

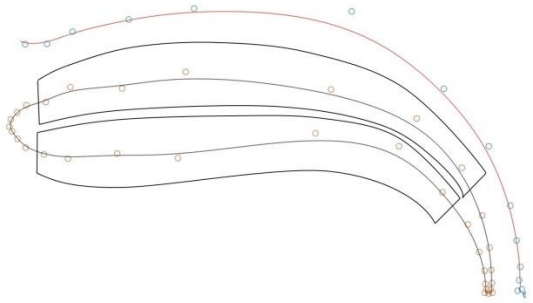

Figure 4-8 Lower Airfoil Constraint

4.3.5 Selection

The DE algorithm is the heuristic search method to solve the minimum problem based on constraints. However, for this work, it is focus on maximum problem of vertical force. So DE algorithm needs to adjust for maximization method. There are two way to construct the maximum to be minimum, reciprocal and negative number, but the reciprocal is nonlinear function, thus, the objective function can be written as:

$$Objective\ Funtion = -F = -(F_L + M_y) \quad [4\text{-}38]$$

In the selection step, it needs to compare every trial vector, and then decides which one can be selected to next generation. Thus in this process, if the trial vector's objective function value is greater than the target vector, the trial vector will be selected to the next generation. After crossover, the trial vector will be written as B-spline Matrix, than generating the new airfoil data file, which can be read by POINTWISE script to generate the case file to FLUENT. The FLUENT writes the results file that can be read by the main code, using the objective function to get the valve and compare to select.

4.3.5 Parameters settings

Parameters settings are often used to measure the pros and cons of evolutionary algorithms. To achieve the desired results, the choice of parameters is critical. Roger Gamperle [42] gave a detailed introduction to the parameter setting techniques of the DE algorithm. The following will talk some of this work's parameter setting. The main parameters of the differential evolution algorithm are: population size NP, scaling factor F, crossover factor CR, and maximum evolution algebra, n.

The scaling factor F is an important parameter for controlling population diversity and convergence. Generally, the value is between 0 and 2. When the F is small, the degree of difference in the population is reduced, and the evolution process does not jump out of the local minimum, leading to premature convergence. When the variation factor F is large, although it is easy to jump out of the local minimum, the convergence speed will be slowed down. Generally available at F=0.5~1.0, in this thesis is 0.7.

The crossover probability CR controls the degree of participation of each dimension of the individual parameters in the crossover, as well as the balance between global and local search capabilities, typically between [0, 1]. The smaller the CR, the smaller the diversity of the population, the easier it is to be deceived, and the premature

convergence. The larger the CR is, the faster the convergence is. However, too large CR may cause convergence to slow down because the disturbance is greater than the group difference. It should generally be chosen between 0.6 and 0.9. Also the larger the CR is, the smaller the F is, setting the CR 0.6.

The population number NP is generally between 5dim and 10dim (dim is the dimension), but not less than 4, otherwise the mutation operation cannot be performed. The larger N is, the stronger the population diversity is, and the optimal solution probability is obtained. But lager NP need calculation time longer, normally choose the number between 20 and 50.

The larger the number of iterations n is, the more accurate of optimum design is, but the calculation time will be need more. So it needs to balance the time and accuracy.

Chapter 5 Results

5.1 Independent study

Grid quality determines the accuracy of CFD simulation. The coarser grid may get the wrong results. As the grid is refined and the time step is refined the spatial and temporal discretization errors, respectively, should asymptotically approaches zero, excluding computer round-off error [43]. So it is important to generate grid fine enough to get accurate results. However, this comes at a cost, larger grid generation and computing time, increase in computational hardware requirements, and need to run the solver with more number of processors. Thus, it is necessary of conducting a grid convergence study.

Some CFD engineers just generate the 2-3 grids with the total volume cell count increasing in some arbitrary manner than perform simulations and declare to achieve a grid independent solution. It is wrong, because GCS requires a systematic orderly variation in spatial resolution in every nook and corner of the domain.

In this situation, to gain some insight into how much grid stretching was needed near the airfoil to obtain a good prediction of the turbulent boundary layer and therefore the aerodynamic coefficients. A grid sensitivity analysis was carried out in the grid direction normal to the surface [44]. Calculating the mesh near the wall properly sized to ensure accurate simulation of the flow field. This calculator computes the height of the first mesh cell off the wall required to achieve a desired y^+ using flat-plate boundary layer theory. Also the S-A turbulent model is more sensitive to the y^+ , though the FLUENT extent the range of it. Choosing y^+ =10, 30, 50, 100 and 200. Pointwise has the y plus calculation by the following equations to get the Wall distance (Δs), Figure 5-1 is the grid

generated by the Pointwise software, the layer number is 35. The mesh numbers are more than 40,000.

$$\mathrm{Re}_x = \rho U_\infty L \mu \quad [5\text{-}1]$$

$$C_f = [2\log_{10}(\mathrm{Re}_x) - 0.65]^{-2.3} \quad [5\text{-}2]$$

$$\tau_\omega = \frac{1}{2} C_f \rho U_{free}^2 \quad [5\text{-}3]$$

$$u_* = \sqrt{\tau_\omega / \rho} \quad [5\text{-}4]$$

$$\triangle s = \frac{y^+ \mu}{\rho u_*} \quad [5\text{-}5]$$

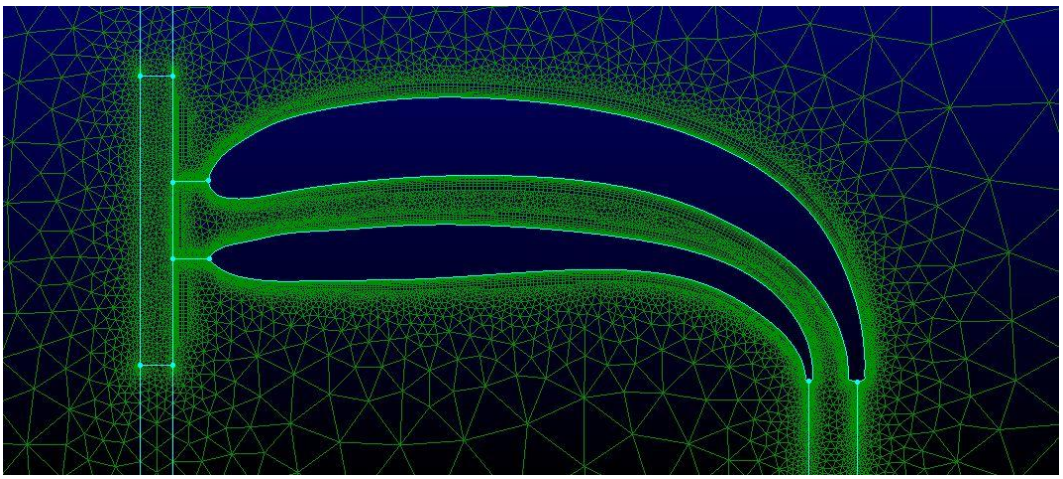

Figure 5-1 Grid

Five different grids were created and a CFD analysis was performed on each of them to obtain the aerodynamic performances. The results obtained with the different y plus grids are shown in table 5-1. All the errors are under 5% compared with the y plus 10. The optimization design is a time consumption process, so each case should spend less time. The y^+ =50 is the best for this case, due to its error is small and the iteration time is not much.

Table 5-1 Grid Convergence Analysis

y plus	Mesh No.	F_L (N)	Q (kg/s)	Velocity (m/s)	M_y (N)	Total (N)	Error	Iteration No.
10	57066	1310.05	-12.890	102.134	1612.77	2922.83		2500
30	50430	1318.14	-12.888	103.512	1634.27	2952.41	1.01%	2000
50	48951	1320.17	-12.894	103.840	1640.19	2960.37	1.28%	1100
100	41195	1332.57	-12.886	105.645	1667.67	3000.24	2.65%	900
200	40795	1339.76	-12.871	107.120	1688.96	3028.73	3.62%	700

5.2 Baseline performance

The vertical force is combined with F_L that is the sum of pressure integration and viscous force and M_y . The propeller and ducted fan contribute to F_L and M_y respectively.

Because the nozzle is close to the propeller, the higher speed flow will interfere with the propeller's airflow, also if the flow of fan is higher than propeller, it also can suck some of the flow that goes to the airfoil into the fan, different conditions need to simulation to find the effects.

When the ducted fan's velocity is the same, changing the propeller's velocity, doesn't affect the momentum force much as shown in the table 5-2, so the propeller does not interfere with the ducted fan, but when the velocity of the propeller is greater than the ducted fan, it can slightly reduce the momentum that is generated by ducted fan.

Table 5-2 Results of Changing the Velocity of Propeller

Ducted Fan (m/s)	Propeller (m/s)	F_L (N)	Q (kg/s)	Velocity (m/s)	M_y (N)	Total (N)
50	20	1236.430	-12.894	103.850	1640.348	2876.777

Table 5-2—*Continued*

50	30	1431.842	-12.894	103.840	1640.202	3072.044
50	40	1825.338	-12.895	103.720	1638.355	3463.693
50	50	2987.935	-12.894	103.604	1636.418	4624.353
50	60	3614.181	-12.878	101.635	1603.382	5217.563

When the velocity of the propeller is the same, changing the ducted fan velocity, showing in the table 5-3, and the strange thing is that the F_L caused by the propeller changes. At the condition of 40 m/s of ducted fan and 20 m/s of the propeller, the F_L is 890.18652 N, when increasing the fan's velocity to 50 m/s, the F_L also increased to 1236.4299. For the airfoil, if the flow does not separate, the faster of upper airfoil and the slower of lower airfoil will get the more F_L according to Bernoulli's principle. Figure 5-2 is the velocity contour of that illustrates the reasons. When the velocity between the gap is acceleration at the end of the airfoil, twice of inlet. For the lower surface of the lower airfoil the high speed velocity is like the wall prohibits the flow to go to the trailing edge, however, for the upper surface of upper airfoil, the flow will acceleration with the high speed airflow that ejects from the gap. In addition, due to the suction of the fan, it will reduce the speed of propeller at begin, so the 40 is less than 50, the airflow at the lower surface flow will be different. As the figure 5-2 show, the 40 m/s figure the upper is faster than and the lower is less than . That's why when increasing the fan velocity will also case the F_L increases.

Table 5-3 Results of Changing the Flow Rate of Ducted Fan

Ducted Fan (m/s)	Propeller (m/s)	F_L (N)	Q (kg/s)	Velocity (m/s)	M_y (N)	Totoal (N)
30	20	585.051	-7.740	62.037	588.215	1173.266

Table 5-3—*Continued*

40	20	890.187	-10.320	83.007	1049.333	1939.520
50	20	1236.430	-12.894	103.850	1640.348	2876.777

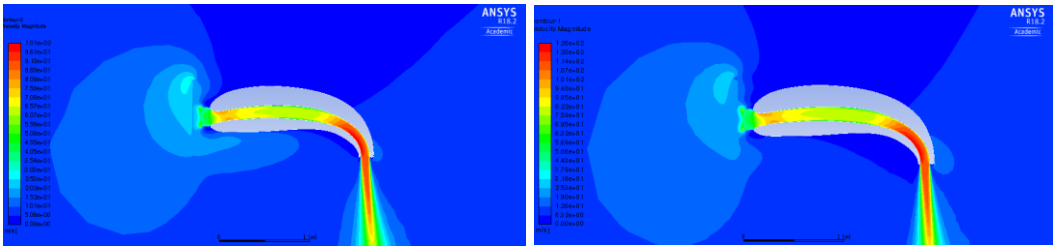

Figure 5-2 40 m/s (left) and 50 /s (right) Velocity Contour

The weight of VTOL is 300 kg, normally the Thrust/Weight is 1.15 or above [1], so the vertical force should be at least 3381 N. Because the airflow that is generated by the ducted fan is faster than propeller, setting the velocity of propeller is half of the fan. The table 5-4 shows that only when the ducted fan velocity is 50 m/s and the propeller velocity is 25m/s, which is better.

Table 5-4 Results of Changing the Both Flow Rate

Ducted Fan (m/s)	Propeller (m/s)	F_L (N)	Q (kg/s)	Velocity (m/s)	M_y (N)	Total (N)	Vertical Force (N)
30	15	510.816	-7.740	62.083	588.639	1099.455	1979.019
40	20	890.187	-10.320	83.007	1049.333	1939.520	3491.135
50	25	1320.175	-12.894	103.840	1640.195	2960.370	5328.666

When changing AOA (Angle of Attack), the lift coefficient of airfoil will change before the airfoil stall. At this design the propeller is the inflow generation, so change the angle of the propeller is to change the AOA. Table 5-5 shows the force changes with the different AOA of propeller at the condition of the ducted fan's velocity is 50 m/s, the

propeller's velocity is 25 m/s. Not like the normal airfoil, when increasing the AOA, the F_L decreases.

Table 5-5 Force Changes with the Different AOA ($V_{fan} = 50m/s$, $V_{prop} = 25m/s$)

AOA (°)	F_L (N)	Q (kg/s)	Velocity (m/s)	M_y (N)	Total (N)
-4	1366.084	-12.895	103.697	1637.976	3004.060
-2	1358.415	-12.894	103.688	1637.827	2996.242
2	1309.545	-12.894	103.687	1637.806	2947.351
4	1288.623	-12.894	103.686	1637.787	2926.410

In the real environment, sometimes it has the wind. At this situation, the 0.2 m/s was set for freestream. The lift force is 1372.07 N, increased 2%. Figure 5-3 is the velocity contour that shows that the wind is a benefit for the F_L .

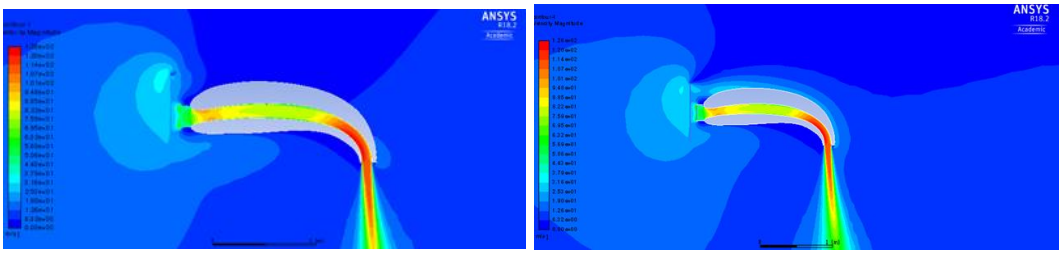

Figure 5-3 0 m/s of freestream (left) and 0.2 m/s of freestream Velocity Contours

According to analysis of the baseline airfoil, choosing the propeller velocity as 25m/s, the fan velocity is 50 m/s and the AOA of propeller are 0° and -4 ° as the two conditions for optimization, although higher velocity of propeller can generated more F_L, they are hard to reality due to the contemporarily technology.

5.3 Test 1

Although the goal of DE code is to find the optimal design, it cannot guarantee the optimization algorithm would find the optimum design. In other words, it was to find the improved design that was able to achieve better performance than the baseline geometry. The first test is at the condition of $V_{fan} = 50m/s$, $V_{prop} = 25m/s$. In the first set, the NP is 20, and the iteration is 45, to prove the convergence, set another trail run, the NP is 24. Each case ran in the desktop computer for 1 week but when ran on the cluster, it just needed 24 to 35 hours.

5.3.1 Results

Figure 5-4 is the initial populations. The two cases are different due to the random algorithm. Figure 5-5 is the convergence, which is value of objective function during the optimization process. At each iteration, the current value is compared with the former, if it is not greater than the former value, the current airfoil control points would replace the former control points to generate the next population. If the value of the function does not change when iterations continue, it is converged, which means the vertical force cannot be improved any more. Figure 5-6 shows the optimized geometry for both trails. The maximum vertical forces of the two trails are 3058.43 N and 3065.28 N respectively after 45 iterations, although the two valves are slightly different, they are converged. Because the second run is better, choosing this to compare with baseline.

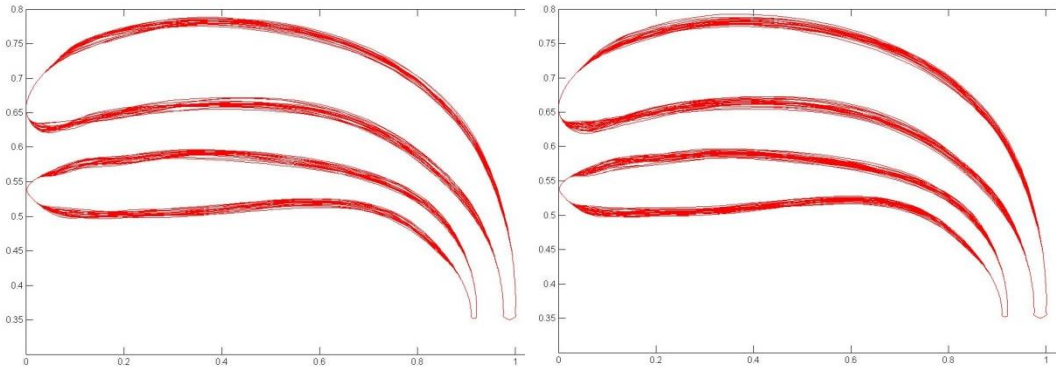

Figure 5-4 Initial Populations

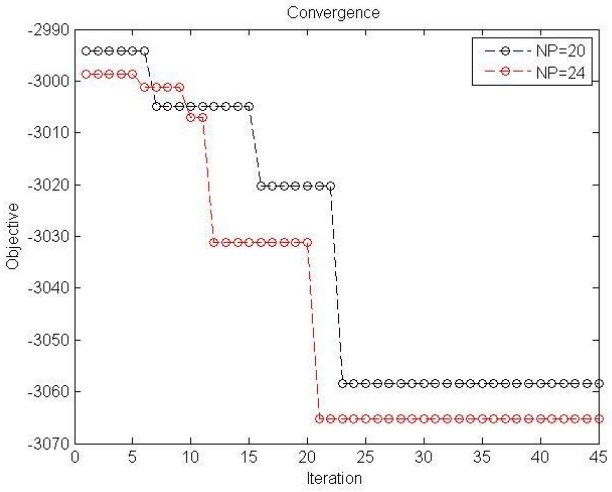

Figure 5-5 Convergence

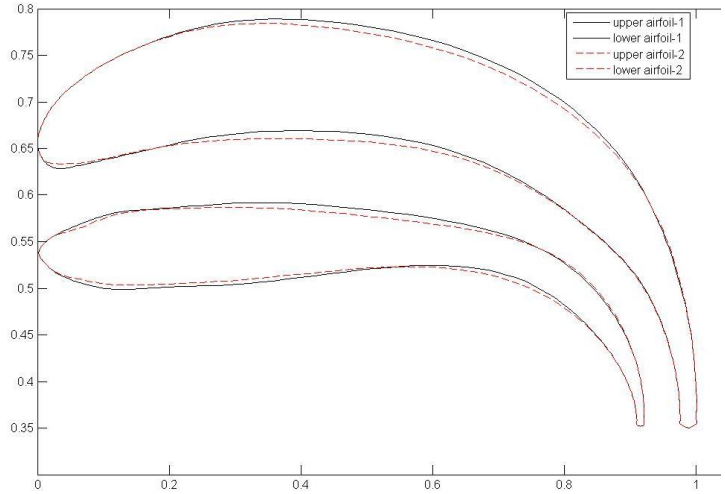

Figure 5-6 Airfoil Shape of Two Runs

5.3.2 Comparison

The vertical force of the optimized airfoil is 3065.28 N; the original is 2960.37 N, increasing 105 N, about 3.55%. The parameters of the airfoils are shown in Figure 5-7. Between the gap, the shape is not the smooth as the airfoil shape, however, the upper of the upper airfoil and the lower of the lower airfoil are smoother than original. The pressure coefficient contours and velocity contours are shown in figure 5-8 and 5-9, which illustrate the reasons. At the beginning of the airfoil, the optimized airfoil the shrink the gap, also it reduce the gap at the rear of the airfoil, let the airflow accelerate, keeping the airflow with higher speed along the gap, so it slight increase the airflow velocity at the end of the nozzle, which benefits for the airflow of the upper of the upper airfoil and prohibits the lower airflow of lower airfoil more, all of these can contribute to the increasing of F_L. In addition, the upper and lower airfoil form the one whole airfoil, the optimized one increased the camber, which can also increase the pressure integration. The figure 5-9 shows that the smooth airfoil can change the velocity distribution that is better than original.

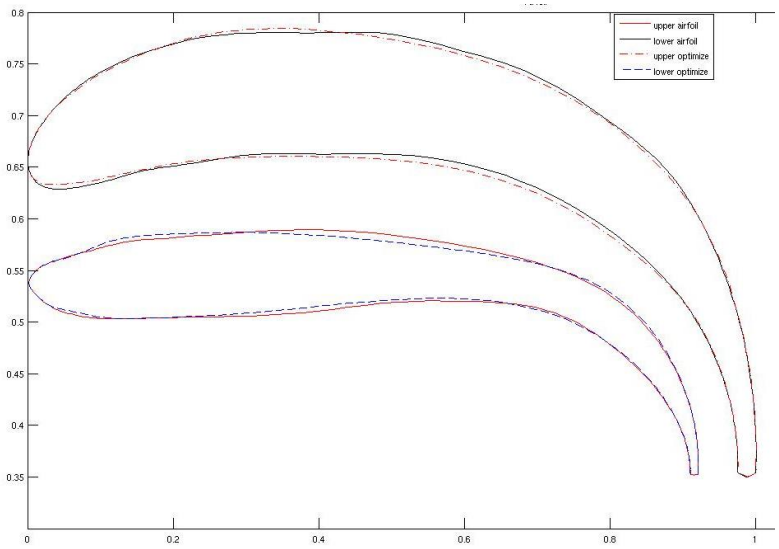

Figure 5-7 Airfoil Shape of Original and Optimized

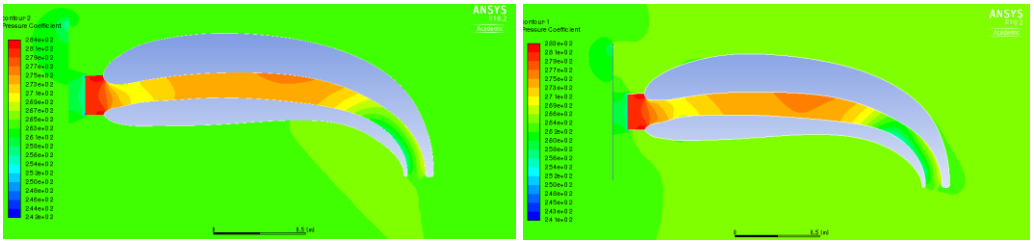

Figure 5-8 Original Airfoil (left) and Optimized Airfoil (right) Pressure Coefficient Contours

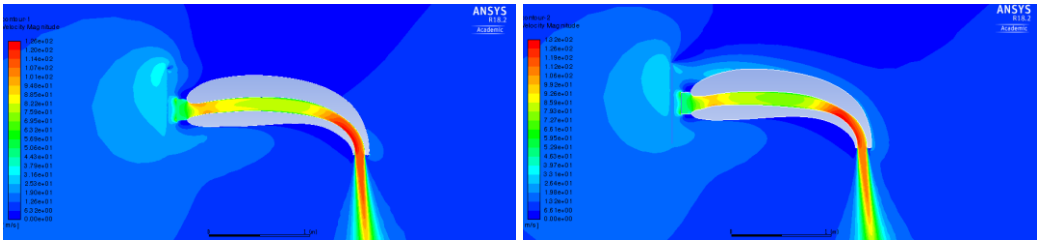

Figure 5-9 Original Airfoil (left) and Optimized Airfoil (right) Velocity Contours

5.4 Test 2

The second test is at the velocity condition, but change the angle of the propeller the AOA is -4°. At the first the set, the NP is 20, and the iteration is 45, to prove the convergence, set another trail run, the NP is 24. Each case ran in the desktop computer for 1 week but when ran on the cluster, it just needed 30 to 40 hours.

5.4.1 Results

Figure 5-10 is the initial populations. The two cases are different due to the random algorithm. Figure 5-11 is the convergence, which is valve of objective function during the optimization process. At each iterate, the current valve compared with the former, if it is not greater than the former value, the current airfoil control points would replace the former control points to generate the next population. If the valve of the function does not change when iterate continues, it is convergence, which means the vertical force cannot be improved any more. Figure 5-12 shows the optimized geometry for both trails. The maximum vertical forces of the two trails are 3259.26 N and 3257.90 N respectively after 45 iterations, although the two valves are slightly different, they are convergence. Because the first run is better, choosing this to compare with baseline.

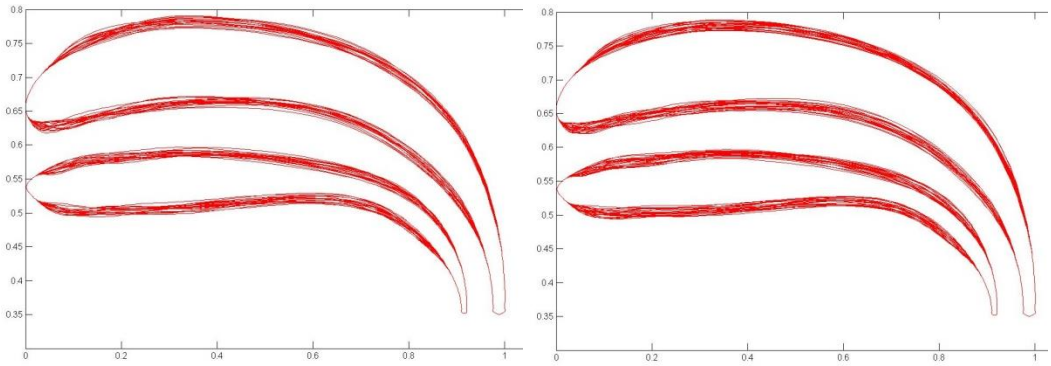

Figure 5-10 Initial Populations

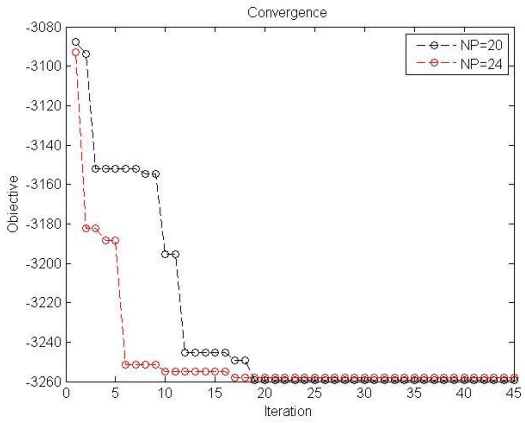

Figure 5-11 Convergence

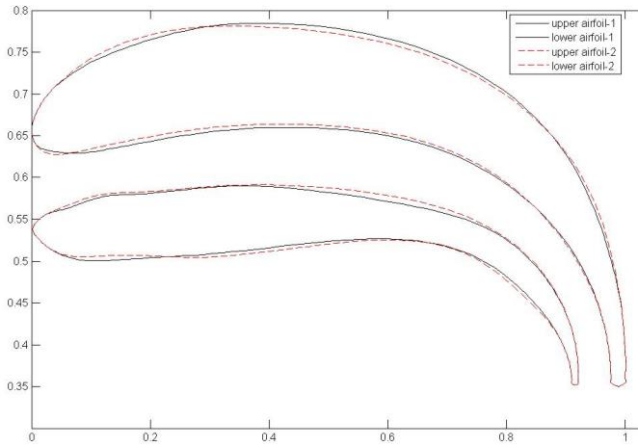

Figure 5-12 Airfoil Shape of Two Runs

5.4.2 Comparison

The vertical force of the optimized airfoil is 3259.26 N; the original is 3004.06 N, increasing 255 N, about 8.50%. The parameters of the airfoils are shown in Figure 5-13. The shape is the smoother than original and reduce the gap at the front part. The pressure coefficient contours and velocity contours are shown in figure 5-14 and 5-15, which illustrate the reasons. At the beginning of the airfoil, the optimized airfoil the shrink almost the whole optimization part of the gap, let the airflow accelerate, keeping the airflow with higher speed along the gap, so it slight increase the airflow velocity at the end

of the nozzle, which benefits for the airflow of the upper of the upper airfoil and prohibits the lower airflow of lower airfoil more, all of these can contribute to the increasing of F_L. In addition, the upper and lower airfoil form the one whole airfoil, the optimized one increased the camber, which can also increase the pressure integration. The figure 5-15 shows that the smooth airfoil can change the velocity distribution that is better than original. Also compare with the test 1, because the propeller has the angle, the airflow are different. The minus amount angel of propeller would benefit for the surface airflow by reducing the ducted fan suction.

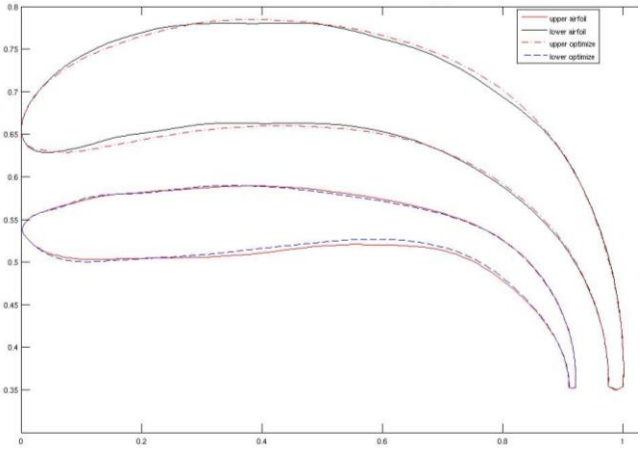

Figure 5-13 Airfoil Shape of Original and Optimized

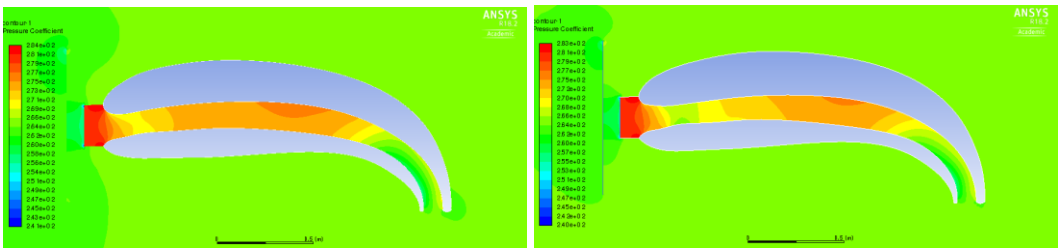

Figure 5-14 Original Airfoil (left) and Optimized Airfoil (right) Pressure Coefficient Contours

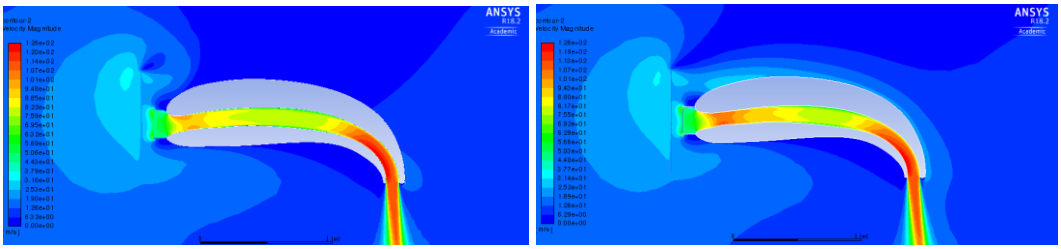

Figure 5-15 Original Airfoil (left) and Optimized Airfoil (right) Velocity Contours

Chapter 6 Conclusions and Future Work

6.1 Conclusion

The single person E-VTOL adopts the both direct lift that is the F_L of the wing and ducted fan with vectoring nozzle and flies at the speed of 120 km/h for 30 minutes, its payload is 120 kg and the total weight is about 300 kg for people to commute around the urban. The E-VTOL is the fly wing configuration with the plate winglet to reduce the drag and landing, its wingspan is 2.5 m, the chord length is 2 m.

The E-VTOL's CG is behind of NP, but it is stable, when slightly disturbance happens, the component of thrust also increases to generate reverse moment to keep the stable.

The direct method is highly reliable and accurate, which is to multiply transpose of N and applying inversion Using matrix equation to get the control points' matrix. When the k= 4 and n=34 is best which has less rounding error.

The propeller does not change the momentum force that generated by the ducted fan, but when the velocity of the propeller is greater than the ducted fan, it can slightly reduce the momentum that generated by ducted fan. However, the ducted fan has great effect on the F_L , the flow of the fan at the end of the airfoil is like the wall prohibits the flow of the lower surface of the lower airfoil to go to the trailing edge, however, for the upper surface of upper airfoil, it accelerates with the upper airflow. At the condition of the ducted fan's velocity is 50 m/s, the propeller's velocity is 25 m/s, when increasing the angle of the propeller, the F_L decreases.

The first test is at the condition of $V_{fan} = 50m/s$, $V_{prop} = 25m/s$, the vertical force of the optimized airfoil is 3065.28 N; the original is 2960.37 N, increasing 105 N, about 3.55%. The second test is at the velocity condition, but change the angle of the propeller

the AOA is -4°. The vertical force of the optimized airfoil is 3259.26 N; the original is 3004.06 N, increasing 255 N, about 8.50%. Though they all do not increase a lot, but it is just the airfoil, if calculate the wing it will be a good increasing.

6.2 Future Work

Due to the time limitation, a lot of works need to be done in the future. First，this work needs to test the sensitivity of the control points, to find which control points they contribute to the shape more. It can also reduce the dimension of the DE but also can get a better airfoil shape.

Secondly, this thesis just optimized the vertical condition, cannot make sure the forward flying situation is the optimization, so it is better to apply the multiobjective optimization design to make sure the forward condition is also good, however, sometimes the it could not meet all objective best, maybe need to sacrifice one objective, it is better to apply the Pareto solution to get the effective and not bad solution.

Last, the 2D design is the simple design, just the first step, it cannot 3D condition, so it is better to optimize the 3D design, and also set the propeller and ducted fan the real airflow fields.

Reference

[1] Holden, Jeff and N. Goel, "Fast-Forwarding to a Future of On-Demand Urban Air Transportation," San Francisco,CA, 2016.

[2] https://www.eaa.org/en/eaa-museum/museum-collection/aircraft-collection-folder/1949-taylor-aerocar.

[3] D. C, "Making Flying Cars Practical: The Terrafugia Master Plan," CEO's Corner.

[4] http://www.bellflight.com/commercial/bell-407gxi.

[5] http://www.bellflight.com/military/bell-boeing-v-22.

[6] R. G. W. J. Fredericks, B. F. McSwain, D. W. Beaton, Klassman and T. Colin R, "Greased Lightning (GL-10) Flight Testing Campaign," 2017.

[7] http://www.dronetechuav.com/offerings.html.

[8] M. Moore, "NASA puffin electric tailsitter VTOL concept," in *In 10th AIAA Aviation Technology, Integration, and Operations (ATIO) Conference*, p.9345. 2010.

[9] "dthi," [Online]. Available: https://gallery.vtol.org/image/dthi.

[10] M. H. Sadraey, Aircraft design: A systems engineering approach, John Wiley & Sons, 2012.

[11] E. Torenbeek, Advanced aircraft design: conceptual design, analysis and optimization of subsonic civil airplanes, John Wiley & Sons, 2013.

[12] D. G. Ullman and V. Homer, "Distributed electric ducted fan wing". U.S. Patent Application Patent 15/374,771, 6 July 2017.

[13] Deere, K. A., J. K. Viken, S. Viken, M. B. Carter, M. Wiese and N. Farr,

"Computational Analysis of a Wing Designed for the X-57 Distributed Electric Propulsion Aircraft," in *In 35th AIAA Applied Aerodynamics Conference*, p.3923.201.

[14] D. Raymer, "Aircraft Design: A Conceptual Approach," American Institute of Aeronautics and Astronautics, Inc., 2012, p. p548.

[15] Vicini, Alessandro and a. D. Quagliarella, "Inverse and direct airfoil design using a multiobjective genetic algorithm," *AIAA journal,* Vols. 35, no. 9, pp. 1499-1505, 1997.

[16] S. Patil, S. Chintamani, R. Kumar and B. Dennis, "Determination of orthotropic thermal conductivity in heat generating cylinder," in *ASME 2016 International Mechanical Engineering Congress and Exposition, American Society of Mechanical Engineer, pp-V011T15A016*, 2016.

[17] S. Patil, S. Chintamani, J. Grisham, R. Kumar and B. and Dennis, "Inverse Determination of Temperature Distribution in Partially Cooled Heat Generating Cylinder," in *ASME 2015 International Mechanical Engineering Congress and Exposition, pp-V08BT10A024-V08BT10A024*, 2015.

[18] O. Fabela, S. Patil, S. Chintamani and B. and Dennis, "Estimation of effective thermal conductivity of porous Media utilizing inverse heat transfer analysis on cylindrical configuration," in *ASME 2017 International Mechanical Engineering Congress*, 2017.

[19] Obayashi, Shigeru and a. S. Takanashi, "Genetic optimization of target pressure distributions for inverse design methods," *AIAA journal ,* Vols. 34, no. 5, pp. 881-886, 1996.

[20] J. Hager, S. Eyi and a. K. LEE, "Multi-point design of transonic airfoils using optimization," in *In Guidance, Navigation and Control Conference, p. 4225.*, 1992.

[21] Jameson, L. M. Antony and a. N. A. Pierce, "Optimum aerodynamic design using the Navier–Stokes equations," *Theoretical and computational fluid dynamics,* Vols. 10, no. 1-4 , pp. 213-237, 1998.

[22] Reuther, James and a. A. Jameson, "Aerodynamic shape optimization of wing and wing-body configurations using control theory," in *In 33rd Aerospace Sciences Meeting and Exhibit, p. 123*, 1995.

[23] David, F. Rogers and a. J. A. Adams, Mathematical elements for computer graphics, McGraw-Hill International, 1990.

[24] M. MacLean, "A Windows program for airfoil design using B-splines," 1999.

[25] J. P. Steinbrenner, "Construction of Prism and Hex Layers from Anisotropic Tetrahedra," in *In 22nd AIAA Computational Fluid Dynamics Conference, p. 2296*, 2015.

[26] R. H. Pletcher, J. C. Tannehill and a. D. Anderson, Computational fluid mechanics and heat transfer, CRC Press, 2012.

[27] v. Leer, Bram and a. K. G. Powell, "Introduction to Computational Fluid Dynamics," *Encyclopedia of Aerospace Engineering,* 2010.

[28] T. J. Baker, "Mesh generation: Art or science?," *Progress in Aerospace Sciences,* Vols. 41, no. 1, pp. 29-63, 2005.

[29] https://www.pointwise.com/theconnector/2011-July/T-Rex-Hybrid-Meshing-Pointwise.html.

[30] http://www.pointwise.com/glyph2/files/Glyph/cxx/GgGlyph-cxx.html.

[31] G. K. Batchelor, An introduction to fluid dynamics, Cambridge university press, 2000.

[32] J. H. Ferziger and a. M. Peric, Computational methods for fluid dynamics, Springer

Science & Business Media, 2012.

[33] "ANSYS Fluent 15 Theory Guide," November 2013.

[34] P. Spalart and S. and Allmaras, "A one-equation turbulence model for aerodynamic flows," in *In 30th aerospace sciences meeting and exhibit, p439*, 1992.

[35] "ANSYS Fluent 15 User's Guide," 2014.

[36] W. J. M. Rankine, "On the mechanical principles of the action of propellers," *Transactions of the Institution of Naval Architects,* vol. 6, 1865.

[37] P. M. Goorjian, "An invalid equation in the general momentum theory of actuator disk," *AIAA Journal,* Vols. 10, no. 4, pp. 543-544, 1972.

[38] J. H. Holland, "Genetic algorithms and the optimal allocation of trials," *SIAM Journal on Computing,* Vols. 2, no. 2, pp. 88-105, 1973.

[39] R. Stom and a. K. Price, "Differential Evolution–A simple and efficient adaptive scheme for global optimization over continuous spaces," Technical Report, TR-95.012, 1995.

[40] Storn, Rainer and a. K. Price, "Differential evolution–a simple and efficient heuristic for global optimization over continuous spaces," *Journal of global optimization,* Vols. 11, no. 4, pp. 341-359, 1997.

[41] Corne, David, M. Dorigo, F. Glover, D. Dasgupta, P. Moscato, R. Poli and a. K. V. Price, "An Introduction to Differential Evolution," in *New ideas in optimization*, McGraw-Hill Ltd, 1999, pp. 79-108.

[42] Gämperle, Roger, S. D. Müller and a. P. Koumoutsakos, "A parameter study for differential evolution," *Advances in intelligent systems, fuzzy systems, evolutionary computation,* Vols. 10, no. 10 , pp. 293-298, 2002.

[43] https://www.grc.nasa.gov/www/wind/valid/tutorial/spatconv.html..

[44] Qin, Ning, A. Vavalle, A. L. Moigne, M. Laban, K. Hackett and a. P. Weinerfelt, "Aerodynamic considerations of blended wing body aircraft," *Progress in Aerospace Sciences,* Vols. 40, no. 6, pp. 321-343, 2004.

[45] T. J. Carrigan, B. H. Dennis, Z. X. Han and B. P. Wang, Aerodynamic shape optimization of a vertical-axis wind turbine using differential evolution, ISRN Renewable Energy 2012 (2012).

Biographical Information

Jie Hua was born in Gaoyou, China. He got the bachelor degree of Engineering in Aircraft Design and Engineering in Zhengzhou University of Aeronautics, China at 2016. After that he became an assistant teacher in Huanghe Jiaotong University, his duties were to teach some courses, such as introduction to aeronautics and astronautics, aerodynamic and charge for UAV Subject and laboratory constructions. He hold the certification of teacher's qualification license of higher education of China, and he is a member of Aero Sports Federation of China. His research interests are Optimization, CFD, VTOL Aircraft Design, Aerodynamic Configuration Design, Numerical Simulation of Aircraft and Propeller and Multidisciplinary Design, UAV Design and Test. He plans to establish a startup company which is to design VTOL aircraft and UAV for logistics.